# An ER-resident calcium binding protein modulates egress of malaria parasites from erythrocytes

Manuel A. Fierro[1,2], Miryam A. HortuaTriana[1], Carrie F. Brooks[1], Beejan Asady[1], Catherine Li[1], Silvia N.J. Moreno[1,2], and Vasant Muralidharan[1,2]

[1]Center for Tropical and Emerging Global Diseases

[2]Department of Cellular Biology

University of Georgia, Athens, GA, USA

Address correspondence to Vasant Muralidharan, vasant@uga.edu

## Abstract

Calcium signaling pathways coordinate the lifecycle progression of apicomplexan parasites, specifically playing a key role in egress from host cells. The main $Ca^{2+}$-signaling hub in these divergent eukaryotic parasites is presumed to be the endoplasmic reticulum (ER); however, no proteins involved in $Ca^{2+}$-signaling have been identified in the ER of these deadly human parasites. In this study, we explored the role of the Endoplasmic Reticulum-resident Calcium-binding protein (ERC) in the lifecycle of two apicomplexan parasites, *Toxoplasma gondii* and *Plasmodium falciparum*. We find that the *Toxoplasma* ortholog (TgERC) plays a role in the storage of $Ca^{2+}$ in the ER but is dispensable for the asexual lytic cycle. On the other hand, the *Plasmodium* ortholog (PfERC) is essential for asexual growth but not required for $Ca^{2+}$ storage, organelle biogenesis, or protein trafficking. Instead, knockdown of PfERC inhibits parasite egress and invasion. Our results show that PfERC is critical for the rupture of the parasitophorous vacuole membrane, which is the first step in the egress of malaria parasites from erythrocytes. Surprisingly, PfERC knockdown does not affect the $Ca^{2+}$-dependent autoprocessing of the key egress protease, SUB1, but knockdown inhibits the second proteolytic maturation of SUB1 that occurs during its secretion from exoneme vesicles. We have therefore identified the first ER-resident protein in *Plasmodium* that modulates egress of malaria parasites.

## Introduction

Members of the phylum *Apicomplexa* are responsible for severe human diseases such as malaria, toxoplasmosis, and cryptosporidiosis. Together, this group of obligate intracellular parasites causes several hundred million infections every year and remains one of the major drivers of infant mortality (1-4). In fact, malaria results in nearly half a million deaths each year and most of the mortality is attributed to one species, *Plasmodium falciparum*. All the clinical symptoms of malaria are directly correlated to the invasion and lysis of the host red blood cells by these parasites. Malaria remains a vast health and economic burden in susceptible parts of the world and, despite continuous attempts for eradication and control, there is no effective vaccine and resistance has emerged to all existing drugs (5-8). This highlights the importance of understanding the factors that control the intracellular growth and development of the parasite, which will lead to the identification of key targets for antimalarial drug development.

Egress and invasion of apicomplexan parasites are ordered and essential processes which are regulated by signaling pathways dependent upon the second messengers, cGMP and $Ca^{2+}$ (9-13). Upon invading the host cell, the parasites create and reside within a host-derived vacuole called the parasitophorous vacuole (PV). Within this vacuole, the parasites grow and divide into daughter cells, called merozoites in *Plasmodium*, which must egress from the host cell to complete the life cycle. This event is triggered by the activation of a cGMP dependent protein kinase (PKG) and the inhibition of PKG activity blocks egress (10, 14, 15). $Ca^{2+}$-signaling also induces egress although it is uncertain whether this pathway works downstream (11) or synergistically with cGMP signaling (10, 16, 17). For example, studies have shown that blocking the release of $Ca^{2+}$ from intracellular stores using cell permeable $Ca^{2+}$ chelators blocks egress in malaria parasites (17-19). It has been suggested that this release of $Ca^{2+}$ into the cytoplasm comes from the parasite ER; however, the parasite genome lacks identifiable orthologs of ligand-gated $Ca^{2+}$ channels such as the inositol 1,4,5,-triphosphate or ryanodine receptors (20). Increase in cytoplasmic $Ca^{2+}$ is thought to activate calcium dependent protein kinases (CDPKs) resulting in release of egress-related vesicles (16, 21).

In malaria parasites, these egress-related vesicles contain specific proteases that are proteolytically processed and activated, perhaps upon release into the PV (22-24).

For example, one such pivotal enzyme is the serine protease, Subtilisin 1 (SUB1), which undergoes two cleavage events. First, the zymogen undergoes $Ca^{2+}$ dependent autoprocessing in the ER (25, 26) and then, it is cleaved again by the recently identified aspartic protease, Plasmepsin X (PMX), probably during its secretion into the PV (23, 24). The proteolytic cleavage and activation of SUB1 is understood to be the point of no-return as the release of SUB1 into the PV results in the rapid (~10 minutes) breakdown of the parasitophorous vacuole membrane (PVM) (22, 27). Then, substrates of SUB1 such as merozoite surface protein 1 (MSP1) and serine-repeat antigen 6 (SERA6) help breakdown the RBC cytoskeleton and the RBC membrane (RBCM) (28, 29). Once egress is completed, the merozoites subsequently invade fresh RBCs to start the cycle again. Like egress, invasion requires specific secretory events such as fusion of micronemes to the merozoite membrane and secretion of rhoptry contents into the host cell, which provides the ligand-receptor pair essential for driving the parasite into the host cell (30, 31).

The parasite endoplasmic reticulum (ER) is thought to play a key role in egress and invasion of daughter merozoites. The putative functions of the parasite ER during these lifecycle stages, include biogenesis of the specific egress and invasion related organelles, transporting proteins to these organelles, and propagating $Ca^{2+}$ signals essential for egress and invasion (32, 33). However, none of the proteins responsible for these ER-related functions during egress and invasion of apicomplexan parasites have been identified. We hypothesized that an ER-resident calcium binding protein (ERC) that is conserved in both *P. falciparum* (PfERC: PF3D7_1108600) and *T. gondii* (TgERC: TGME49_229480) plays a role in the $Ca^{2+}$ signaling function of the parasite ER. In malaria parasites, this protein has been shown to bind calcium (34). However, the biological function of ERC is unknown in either apicomplexan parasite.

To address this, we used a ribozyme-based conditional knockdown system to study the role of PfERC in the asexual lifecycle *P. falciparum*, and we used a knock-out approach to study the role of TgERC in the biology of *T. gondii*. We characterized the role of both $Ca^{2+}$ binding proteins, PfERC and TgERC, and propose a model for their potential roles in $Ca^{2+}$ signaling and in the life cycle of both parasites. This is the first ER resident

protein identified in *P. falciparum* that is critical for the egress of malaria parasites from human red blood cells.

## Results

### PfERC and TgERC are EF-hand containing proteins localized in the ER

PfERC (PF3D7_1108600) and TgERC (TgME49_229480) are proteins related to the CREC (Calumenin, Reticulocalbin 1, ERC-55, Cab-45) family of proteins, which are characterized by the presence of multiple EF-hands and localize in various parts of the secretory pathway (35) (Figure 1A and Supplementary Figure 1). Like CREC members in other organisms, both PfERC and TgERC contain a signal peptide, multiple EF-hands, and an ER-retention signal (Figure 1A). However, TgERC differs from its *Plasmodium* homolog in that it only contains 5 EF-hands while PfERC contains and extended C-terminus that may contain a 6$^{th}$, though degenerate, EF-hand (residues 314-325) (Supplementary Figure 1) (34). Since both proteins have an ER-retention signal they are predicted to reside within the lumen of the ER.

### Generating conditional mutants of PfERC

In order to determine the biological role of PfERC, we used CRISPR/Cas9 gene editing to generate mutant parasite lines where the endogenous locus of PfERC was tagged with the conditional knockdown system employing the inducible ribozyme *glmS* or the inactive version of the ribozyme, *M9* (termed PfERC-*glmS* and PfERC-*M9* respectively) (Figure 1B and 1C) (36). Western blot and PCR analysis of PfERC-*glmS* and PfERC-*M9* parasite clones from two independent transfections demonstrate the correct insertion of the HA tag and the *glmS/M9* ribozymes at the PfERC locus (Figure 1D and 1E). Co-localization of PfERC with an ER marker also confirmed its sub-cellular localization to this organelle (Figure 1F).

### PfERC is essential for asexual growth and for schizont to ring transition

To determine if PfERC was essential for intraerythrocytic survival, we grew asynchronous PfERC-*glmS* and PfERC-*M9* parasites in the presence of glucosamine (GlcN), which activates the *glmS* ribozyme leading to mRNA cleavage (Figure 1B).

Western blot analysis shows that this leads to a reproducible reduction of PfERC expression in PfERC-*glmS* parasites while there is no reduction of protein levels in PfERC-*M9* parasites grown under identical conditions (Figure 2A-B). Importantly, this reduction in PfERC levels inhibited the asexual expansion of PfERC-*glmS* parasites, while there was no effect on the growth of PfERC-*M9* parasites (Figure 2C). The response of PfERC-*glmS* parasites was dose-dependent upon GlcN (Supplementary figure 2A)

Since our data show that PfERC was essential for growth within the host RBC, we used synchronous parasites to determine which asexual stage was affected by knockdown. We added GlcN to synchronized schizonts and took blood smears at regular intervals during the intraerythrocytic life cycle to detect morphological development of the asexual stages (Figure 2D). Our data show that all intracellular stages developed normally in both PfERC-*glmS* and PfERC-*M9* parasites grown with GlcN (Figure 2D and Supplementary Figure 2B). However, 55hrs after addition of GlcN, the PfERC-*glmS* parasites remained either as morphologically normal schizonts or were observed as daughter merozoites in the extracellular space as well as some that were attached to RBCs (Figure 2D). On the other hand, PfERC-*M9* parasites were able to egress and re-invade fresh RBCs and developed into ring stage parasites (Figure 2D and Supplementary figure 2B).

These data suggest that the knockdown of PfERC resulted in a defect in the conversion from schizonts to rings. Therefore, we induced knockdown and observed the conversion of schizonts into rings via flow cytometry at 44, 48, and 56 h post-addition of GlcN. The data show that over the course of 12 hours, PfERC-*M9* parasites transitioned from schizonts to rings as determined by the ring:schizont ratio while PfERC-*glmS* parasites were unable to convert from schizonts into rings resulting in a drastically reduced ratio (Figure 2E). These data show that there was a delay in the disappearance of the morphologically normal PfERC-*glmS* schizonts over the final few hours of the asexual life cycle compared to PfERC-*M9* schizonts, suggesting that knockdown of PfERC led to a defect in egress (Figure 2F and 2G). Consequently, the delayed egress may lead to reduced numbers of ring stage parasites in PfERC-*glmS* parasites unlike PfERC-*M9* parasites (Figure 2F and 2H).

## PfERC is required for PVM breakdown

Egress of daughter merozoites from the infected RBC is an ordered and rapid process where the PVM breakdown precedes the disruption of RBCM (Figure 3A). Therefore, we analyzed how egress of PfERC-*glmS* parasites was failing during knockdown. We took synchronized PfERC-*glmS* and PfERC-*M9* schizonts and initiated knockdown with addition of GlcN. These schizonts were allowed to reinvade fresh RBCs and proceed through the asexual stages for 48 hours until they developed into schizonts again. Then, these second cycle schizonts were incubated with inhibitors that block key steps during egress of *P. falciparum* (Figure 3A). To ensure synchronized egress, we used reversible inhibitors of PKG, Compound 1 (C1) or Compound 2 (C2), because inhibition of PKG allows merozoites to develop normally but prevents them from initiating egress (Figure 3A) (10, 15). We used flow cytometry to observe PfERC-*glmS* and PfERC-*M9* schizonts after washing off C1 and saw that there was a delay in the egress of PfERC-*glmS* schizonts while the majority (>60%) of the PfERC-*M9* schizonts were able to complete egress within two hours after washout of C1 (Figure 3B). Removal of C1 initiates the breakdown of the PVM followed by RBCM rupture (Figure 3A), suggesting that PfERC-*glmS* parasites fail to breach one of these membranes down despite removal of the PKG inhibitor.

Therefore, we tested whether PfERC knockdown prevented rupture of PVM or if PfERC functioned during RBCM breakdown (Figure 3A). PfERC-*glmS* and PfERC-*M9* schizonts (where knockdown had been initiated in the previous cycle) were incubated with C2 (10, 15) and observed by scanning electron microscopy (SEM) (Figure 3A and 3C). We observed that parasites treated with C2 were morphologically identical and had developed into mature schizonts within the PVM inside the RBC (Figure 3C). Then, we washed C2 from the parasites and observed these schizonts after 30 mins by SEM (Figure 3C). During this time period, PfERC-*M9* schizonts were able to initiate egress after removal of C2 and we observed free merozoites attached to the RBC as well as clusters of merozoites that had broken out of the PVM but were contained by a collapsed RBCM wrapped around them (Figure 3C). In contrast, the PfERC-*glmS* schizonts were still stuck within the RBC and looked identical to the C2 arrested schizonts, suggesting that they had not initiated egress even though PKG was no longer inhibited (Figure 3C).

These data suggest that knockdown of PfERC blocks egress at an early step, perhaps blocking the rupture of the PVM (Figure 3C).

We directly observed if breakdown of the PVM was impacted by knockdown of PfERC using transmission electron microscopy (TEM) (Figure 3D). Knockdown was induced by adding GlcN to PfERC-*glmS* and PfERC-*M9* schizonts and these parasites were allowed to go through one asexual cycle and develop into schizonts again 48hrs later. These schizonts were prevented from completing egress using the irreversible cysteine protease inhibitor, E64 (Figure 3A). This inhibitor blocks the breakdown of the RBCM but allows both the breakdown of PVM and poration of the RBCM, which results in the loss of the electron dense contents of the infected RBC (Figure 3A) (15, 29, 37). Our results show that the PfERC-*M9* schizonts were able to break down the PVM as well as proceed with the poration of the RBCM after an 8-hour incubation with E64, while the PfERC-*glmS* mutants were unable to proceed through the first step of egress and failed to rupture the PVM (Figure 3D). Overall, these data demonstrate that PfERC function is critical for the breakdown of the PVM (Figure 3C and 3D).

Generating knockouts of TgERC

We hypothesized that the ortholog of PfERC in the related apicomplexan parasite, *T. gondii,* may play a similar in the egress of this parasite from its host cell. Therefore, we studied the biological role of TgERC by disrupting the transcription of the *tgerc* gene using CRISPR/Cas9 gene editing to insert the selection marker gene, dihydrofolate reductase (DHFR), in the *tgerc* locus (38, 39) (Figure 4A). Insertion of this gene into the *tgerc* locus interfered with the synthesis of the correct transcript and allowed the selection of clonal populations with pyrimethamine. The mutant *Δtgerc* was isolated by limiting dilution, and a PCR product of 6.1 kb obtained from the mutant parasites DNA indicated the insertion of the marker in the predicted locus (Figure 4B). This fragment was only amplified from DNA of mutants while a fragment of 2.9kb was amplified from parental cells, which correspond to the intact locus of *tgerc* (Figure 4B).

In order to verify the localization of TgERC, we cloned and expressed TgERC in *E. coli* and the purified recombinant protein to immunize mice for the generation of specific antibodies. Western blot analysis using this antibody showed the presence of a ~38kDa

band corresponding to TgERC in the parental (RH) parasites but absent in the Δ*tgerc* mutants (Figure 4C). Furthermore, IFAs using this antibody showed that TgERC localized predominantly to the endoplasmic reticulum in both extracellular and intracellular tachyzoites (Figure 4D).

TgERC is required for $Ca^{2+}$ storage but PfERC is not

To determine whether TgERC was essential for the lytic cycle of the parasites, we performed plaque assays comparing growth of RH wild type with *Δtgerc* (Figure 4E). Our data show that the mutant parasites were able to form plaques about the same size as the controls (Figure 4F). These data suggest that unlike PfERC, TgERC was not required for egress from the host cell nor was it essential for the lytic cycle of *T. gondii*.

We next tested the if TgERC had any role in the storage of $Ca^{2+}$ by testing for increases in cytoplasmic $Ca^{2+}$ in response to thapsigargin. This inhibits the SERCA-$Ca^{2+}$ ATPase, exposing leakage of $Ca^{2+}$ from the ER into the cytoplasm as detected by fluorescence changes in parasites loaded with the $Ca^{2+}$ indicator Fura-2AM (Figure 4G-J) (40, 41). We observed that the cytoplasmic $Ca^{2+}$ increase in the *Δtgerc* mutants after adding thapsigargin was not significantly different than the response obtained under identical conditions when using wild type parasites (Figure 4G). However, when we performed the same experiment in the presence of extracellular $Ca^{2+}$ (Figure 4I), the response to thapsigargin in *Δtgerc* tachyzoites was significantly reduced. The reduced response in the *Δtgerc* parasites indicates that the ER of these parasites is unable to store $Ca^{2+}$ as efficiently as the wild type. This indicates that TgERC is part of the ER machinery involved in storing $Ca^{2+}$. However, it is evident that other mechanisms are in play since the parasites are still able to grow normally (Figure 4E-F).

Since knockout of TgERC resulted in defects in $Ca^{2+}$ storage in the ER of *T. gondii* (Figure 4I and 4J), we hypothesized that PfERC is required for egress because it plays a similar role in *P. falciparum* and does not have redundant mechanisms like *T. gondii* that compensate for the lack of TgERC. To test this hypothesis, synchronized PfERC-*glmS* and PfERC-*M9* schizonts were incubated with GlcN and allowed to proceed through one asexual cycle until they formed schizonts again. The second cycle schizonts were isolated using saponin lysis and loaded with Fluo-4AM to measure cytosolic $Ca^{2+}$ (Supplementary

Figure 3A). To assess if the storage of $Ca^{2+}$ in the ER of the parasite was affected by knockdown of PfERC, we added the SERCA-$Ca^{2+}$ ATPase inhibitor Cyclopiazoic acid (CPA) to these saponin-isolated parasites (Supplementary Figure 3A and 3B) (42). Inhibiting the SERCA-$Ca^{2+}$ ATPase allows $Ca^{2+}$ stored in the ER to leak into the cytoplasm, which results in a detectable change in the fluorescence of Fluo-4AM (Supplementary Figure 3B). Our measurements show that there was no difference in the amount of $Ca^{2+}$ that leaked from the parasite ER, upon SERCA-$Ca^{2+}$ ATPase inhibition, between PfERC-*glmS* and PfERC-*M9* schizonts (Supplementary Figure 3B).

To test if there was a defect in $Ca^{2+}$ storage in neutral stores, we used the ionophore, Ionomycin, which releases $Ca^{2+}$ from all neutral stores in the cell and measured the release of $Ca^{2+}$ into the cytoplasm of PfERC-*glmS* and PfERC-*M9* schizonts. The parasites were isolated as described above and the changes in cytoplasmic $Ca^{2+}$ were measured using Fluo-4AM (Supplementary Figure 3A and 3C). Again, we did not observe any difference in the amount of $Ca^{2+}$ released into the cytoplasm of PfERC-*glmS* and PfERC-*M9* schizonts treated with ionomycin (Supplementary Figure 3C). These data suggest that the availability of free $Ca^{2+}$ in the ER of *P. falciparum* is not affected by knockdown of PfERC. Furthermore, these data suggest that the observed egress defect upon PfERC knockdown was not a result of disequilibrium of $Ca^{2+}$ in the parasite ER.

Efficient SUB1 activation requires PfERC

Electron microscopy data show that knockdown of PfERC prevents the breakdown of the PVM (Figure 3). A key event required for PVM breakdown is the proteolytic processing of SUB1, which starts a cascade that ends in the release of merozoites from the infected RBC (22, 29). Therefore, we tested if knockdown of PfERC affects processing of PfSUB1. This protease is processed twice, once in the ER, where it undergoes a $Ca^{2+}$-dependent autocatalytic processing from its zymogen form (83-kDa) into a 54-kDa semi-proenzyme form (p54) (25, 26, 43). From the ER, SUB1 is transported to the egress-related secretory vesicles, the exonemes, which are secreted into the PV to initiate breakdown of the PV membrane. It is proposed that during secretion of SUB1, it is processed by PMX from its semi-proenzyme form (p54) to its mature form (p47) (23, 24).

The secretion of mature p47 form of SUB1 initiates the breakdown of the PVM (22, 43). We hypothesized that PfERC is required for the first $Ca^{2+}$-dependent autoprocessing of SUB1, in the ER, from the 82-kDa zymogen into the p54 semi-proenzyme.

To test this hypothesis, PfERC-*glmS* and PfERC-*M9* schizonts were incubated with GlcN and allowed to progress through one asexual growth cycle (48 hours) to develop into schizonts again. Lysates from these synchronized schizonts were separated on a Western blot and probed with antibodies against SUB1 (Figure 5A and Supplementary Figure 4A). No change was observed in the $Ca^{2+}$-dependent autoprocessing of the zymogen-form of SUB1 into the semi-proenzyme (p54) form (Figure 5A and Supplementary Figure 4A). Surprisingly, we observed a reproducible and significant decrease in the processing of SUB1 from p54 to the p47 form in PfERC-*glmS* parasites (Figure 5A and 5B). Compared to PfERC-*M9* parasites, there was a >50% decrease in the amount of processed SUB1 (p47) in PfERC-*glmS* parasites (Figure 5B). These data suggest that PfERC is required for the secretion-dependent processing of SUB1 in exoneme vesicles.

Since we observed the presence of some mature SUB1 in PfERC-*glmS* parasites (Figure 5A), we tested if the activity of SUB1 was affected upon knockdown of PfERC by assaying for the processing of a known substrate of SUB1, the merozoite surface protein 1 (MSP1). MSP1 is required for the initial attachment of merozoites onto RBCs and it has been shown that correct processing of MSP1, by SUB1, is also required for efficient egress as it plays a role in breakdown of the RBC cytoskeleton after release from the PVM (28, 44-46). Lysates from synchronized second-cycle PfERC-*glmS* and PfERC-*M9* schizonts, treated as above, were separated on a Western blot and probed using anti-MSP1 antibodies (Figure 5C and Supplementary Figure 4B). Our data show that the there was a ~60% reduction in MSP1 processing in our PfERC-*glmS* parasites as compared to PfERC-*M9* parasites after knockdown (Figure 5C). In fact, we observed that PfERC-*glmS* schizonts had 3 times more unprocessed MSP1 in contrast to PfERC-*M9* schizonts (Figure 5D). These data reveal that knockdown of PfERC leads to defects in SUB1 processing and activity, and consequently, MSP1 processing (Figure 5).

<u>Knockdown of PfERC does not affect protein trafficking or organelle biogenesis</u>

MSP1 is a GPI-anchored merozoite membrane protein that is presumably processed by SUB1 once the protease is secreted into the PV (28, 29). Therefore, we wanted to verify that knockdown of PfERC led to a specific defect in the egress cascade and is not due to a block in protein trafficking via the ER or defects in the biogenesis of egress and invasion related organelles. To address this, we used super resolution structured illumination microscopy (SR-SIM) to observe if there was a difference in the surface expression of MSP1 between PfERC-*glmS* and PfERC-*M9* schizonts upon knockdown of PfERC (Figure 5E). As before, knockdown was initiated in synchronized PfERC-*glmS* and PfERC-*M9* schizonts and after 48 hours, these schizonts were stained with anti-MSP1 antibodies. Our data shows that there was no difference in the trafficking of MSP1 to the surface of developing PfERC-*glmS* or PfERC-*M9* merozoites after knockdown (Figure 5E). In addition, we also tested whether the localization of other egress-and invasion-related proteins that traffic through the ER where affected after knockdown by staining similarly treated schizonts for the micronemal protein AMA1 and the rhoptry-bulb protein RAP1. Our data show that, again, there was no difference in the localization of these proteins in schizonts between PfERC-*glmS* and PfERC-*M9* parasites suggesting that the knockdown of PfERC does not cause a generalized defect in the secretory pathway (Figure 5F&G).

As the ER generates the lipid membranes required for generating organelles essential for egress and invasion, we wanted to see if their biogenesis was inhibited upon knockdown. If true, this could explain the processing defects that we observe for SUB1 and MSP1. We observed E64-treated schizonts (Figure 3A) by transmission electron microscopy and these data show that both micronemes and rhoptries remain morphologically intact in both PfERC-*glmS* and PfERC-*M9* parasites after knockdown was induced (Figure 5H). Successful knockdown was confirmed by the lack of PVM membrane fragments in PfERC-*glmS* parasites, which are present in the PfERC-*M9* parasites, suggesting that PVM rupture occurred normally in the presence of PfERC but not when the protein is knocked down (Figure 5H). These data suggest that the knockdown of PfERC does not lead to defects in organelle biogenesis (Figure 3D and Figure 5H).

## PfERC is required for invasion of merozoites

The synchronized growth assays suggest that knockdown of PfERC inhibits the invasion of merozoites into RBCs (Figure 2D, H and Figure 5C, D). To assess if invasion was reduced upon knockdown, PfERC-*glmS* and PfERC-*M9* schizonts in the second cycle after 48 hours in GlcN, were incubated with the PKG inhibitor, C1, for four hours (Figure 3A). The inhibitor was then washed off and the formation of ring stages was observed over two hours by flow cytometry (Figure 6A). We observed that there was a delay in the formation of ring stages as well as a drastic decrease in the numbers of ring stage parasites formed in PfERC-*glmS* parasites compared to the PfERC-*M9* control (Figure 6A). This could be due to loss of egress or could be a combination of effects on egress and invasion due to PfERC knockdown.

To decouple the egress and invasion phenotypes, we directly measured the efficiency of merozoite invasion (Figure 6B). This was accomplished by incubating second cycle PfERC-*glmS* and PfERC-*M9* schizonts with E-64 and then mechanically releasing the merozoites (Figure 6B) (47). Incubation with E-64 for 8 hours allows for the completion of schizogony and formation of invasion-competent merozoites. These purified merozoites were then allowed to invade fresh RBCs and the invasion rate was quantified using flow cytometry as described previously (Figure 6C) (47). These data show that there was a drastic reduction in the invasion efficiency of PfERC-*glmS* merozoites as compared to the control PfERC-*M9* merozoites, thus demonstrating that knockdown of PfERC led to a defect in invasion as well (Figure 6C).

## PfERC knockdown affects proteolytic processing of AMA1

The reduced invasion of PfERC-*glmS* merozoites could be explained by the reduction in processing of MSP1, which is known to be required for the initial attachment of merozoites to the RBC (44, 45, 48). Invasion of RBCs by *P. falciparum* merozoites requires secretion of contents from another apical organelle, the rhoptries, into the RBC (49-51). Proteins in the rhoptries, like the rhotry-bulb protein, RAP1, require proteolytic processing for their activity (23, 24). Once in the rhoptry, RAP1 is processed by the aspartic protease, Plasmepsin IX (PMIX), from a pro-form (p83) to a mature form (p67) (23, 24, 52, 53). Therefore, we tested if RAP1 processing was affected by knockdown of

PfERC using Western blot analysis (Figure 6F and Supplementary Figure 4C). Our data show that the proteolytic processing of RAP1 was not affected by the knockdown of PfERC (Figure 6G), showing that knockdown does not lead to a generalized defect in the processing of all proteins that traverse through the secretory pathway.

Another key and essential step in invasion of merozoites is the formation of a tight junction between the parasite and the RBC and AMA1 is critical for the formation of this tight junction (30, 31). AMA1 is trafficked from micronemes to the merozoite surface and there it is processed from its pro-form (p83) to its mature form (p66) by an unknown protease (54-56). The proteolytic processing of AMA1 is critical for its function during invasion (57). Therefore, we tested if the processing of the AMA1 was affected upon knockdown of PfERC. As before, after initiating knockdown in synchronized schizonts, we separated lysates from second cycle PfERC-*glmS* and PfERC-*M9* schizonts on a Western blot and probed it with anti-AMA1 antibodies (Figure 6D and Supplementary Figure 4D). We observed a significant reduction in the proteolytic processing of AMA1 upon knockdown (Figure 6D). Indeed, there was a >40% decrease in the processing of AMA1 in PfERC-*glmS* mutants compared to the PfERC-*M9* control (Figure 6E). These data suggest that PfERC is required for the correct processing of AMA1 and therefore, essential for invasion of merozoites into the host RBC.

## Discussion

In this study, we addressed the biological role of a conserved $Ca^{2+}$-binding protein that resides in the lumen of the ER of apicomplexan parasites. We have shown that the *Toxoplasma* homolog, TgERC, is dispensable for *in vitro* growth, and the *Plasmodium* homolog, PfERC, is essential for asexual replication (Figures 2 and 3). Our data show that knockdown of PfERC did not affect the ring and trophozoite development but had a clear effect on the subsequent schizont-to-ring transition (Figures 2D-H, 3B, 6A, and Supplementary Figure 2). Specifically, these data show that PfERC is required for both egress from infected RBCs (Figures 2D, 2G, and 3) and invasion into host erythrocytes (Figures 2D, 2H and 6A-C). This is consistent with data that suggest PfERC may be transcriptionally controlled by the invasion-specific transcription factor PfAP2-I (58). Our data show that knockdown of PfERC leads to defects in the processing of proteins critical

for invasion of merozoites into the host RBC, namely, MSP1 and AMA1 (Figures 5C-D and 6 D-E). However, the observed invasion defect is likely a secondary effect because several proteins critical for invasion are processed during egress (28, 29). Given the limitations of the conditional knockdown system, we cannot tease out a specific role for PfERC in invasion. As invasion occurs rapidly (<2mins), a potential specific invasion-related function of PfERC could be tested using a small molecule that specifically targets PfERC (59). Overall, these data show that PfERC is essential for egress of merozoites from the infected RBC and for invasion of merozoites into the host erythrocyte.

It has been observed previously that the mechanisms at play during egress of daughter parasites from the host cells differs between *Toxoplasma* and *Plasmodium.* This is highlighted by studies showing that orthologs of apicomplexan proteins can serve different functions in their respective organisms. For example, TgCDPK3 is required for egress of *T. gondii* tachyzoites while its *Plasmodium* ortholog, PfCDPK1, is essential for both egress and invasion (60). Similarly, another calcium dependent protein kinase, TgCDPK1, plays a vital role in egress and invasion of *Toxoplasma* tachyzoites but the *Plasmodium* ortholog, PfCDPK4, was shown to be required for the development of sexual stages (60). Additionally, TgSUB1 localizes to micronemes and is used for processing of micronemal proteins that are required for invasion of *T. gondii* into host cells (61). However, PfSUB1 is critical for egress of *Plasmodium* merozoites, localizes to exonemes, and upon secretion into the PV, processes both micronemal and non-micronemal proteins (22, 62). These differences could be related to their development within different host cells. *Plasmodium* prefers the erythrocyte for its asexual expansion and *Toxoplasma* is able to make its home within any nucleated cell. Another factor is the difference in the primary structure of TgERC and PfERC, which possesses an additional putative EF-hand domain compared to its homolog in *T. gondii.* Therefore, it is not surprising that the biological role of TgERC may be different from the function of PfERC. This was evident in the data that suggest that TgERC plays a role in ER $Ca^{2+}$ storage but PfERC may not (Figures 4I, 4J and Supplementary Figure 3). It is interesting to note that there are no orthologues of many $Ca^{2+}$ entry channels such as store-operated channels (ORAI), or their partners such as the ER sensor protein stromal interaction molecule (STIM) in the genome of apicomplexan parasites. Future work on identifying the interacting partners of

454 TgERC may provide some clues as to the identity of putative ER $Ca^{2+}$ sensors that could
455 regulate the function $Ca^{2+}$ entry channels in these divergent parasites.

456 During the formation of daughter merozoites in schizonts, several key egress and
457 invasion related organelles essential for propagation of the infection are generated. The
458 ER is thought to play a key role in the biogenesis of these organelles and the ER is
459 responsible for transporting the essential proteins to these organelles (32, 33). As an ER-
460 resident protein, knockdown of PfERC could affect several ER functions such as protein
461 trafficking, organellar biogenesis, and $Ca^{2+}$ signaling. Therefore, we tested if PfERC
462 functions in the trafficking of proteins required for schizont to ring transition such as MSP1,
463 AMA1, and RAP1. A defect in the secretory pathway would explain the observed
464 deficiencies in the proteolytic processing of SUB1, MSP1 and AMA1, as transport out of
465 the ER is required for their maturation (10, 26, 52, 63). However, super-resolution and
466 electron microscopy experiments showed that trafficking of proteins to the merozoite
467 surface, micronemes, and rhoptries or their biogenesis are not affected (Figures 3D and
468 5E-5H). Likewise, Western blot analysis showed that the proteolytic processing of a
469 rhoptry protein, RAP1, which is processed after transport to the organelle, is not affected
470 by knockdown of PfERC (Figures 5G, and 6F-G) (23, 24). These data show that
471 knockdown of PfERC does not result in a generalized defect in protein trafficking via the
472 ER or in organelle biogenesis.

473 Immunofluorescence microscopy, electron microscopy, and $Ca^{2+}$ measurements
474 ruled out a role for PfERC in $Ca^{2+}$ storage, protein trafficking, or organelle biogenesis
475 (Figures 3D, 5E-G, 6F, 6G and Supplementary Figure 3). Another interesting possibility
476 is that PfERC may play a role the signal-dependent release of $Ca^{2+}$ from the ER. PfERC
477 is a member of the CREC family of proteins and other members of this family are known
478 to play key roles in the function of ligand-gated $Ca^{2+}$ channels. For example, calumenin
479 and reticulocalbin 1 have been shown to interact with the Ryanodine and $IP_3$ receptors,
480 respectively, and regulate their function (64, 65). It has also been suggested that some
481 CREC members serve as $Ca^{2+}$ sensors in the ER as they exhibit calcium-dependent
482 structural changes (66, 67). This is difficult to test in *Plasmodium* since there are no clear
483 homologs for a ligand-dependent $Ca^{2+}$ channel in its genome (20). At present, $Ca^{2+}$
484 measurements in *P. falciparum* require lysis of the RBCM that results in loss of the RBC

485 contents and this complicates any conclusions reached from egress-related experiments
486 since it is unknown if components in the RBC are essential for the signaling pathway
487 required for egress. However, this may be addressed by using less invasive approaches
488 that do not require lysis of the RBCM such as genetically-encoded $Ca^{2+}$ indicators (GECI)
489 to measure changes in ER $Ca^{2+}$ during egress or by studying the egress-related roles of
490 proteins that interact with PfERC.

491 Consistent with a role for PfERC in signal-dependent release of $Ca^{2+}$ from the ER,
492 we observed that knockdown resulted in a clear defect in egress (Figures 2G, 3, and 5A-
493 D). Egress is a rapid process and the genetic mechanisms in the ER of apicomplexan
494 parasites that control the signal-dependent release of $Ca^{2+}$ from the ER are unknown.
495 Our data supports a model where PfERC functions in the signaling pathway that releases
496 $Ca^{2+}$ from the ER required for the egress of merozoites from the infected RBC. This model
497 would also predict that PfERC plays a role in the release of $Ca^{2+}$ from the ER, such that
498 in the absence of PfERC, the ER is unable to release $Ca^{2+}$ upon the requisite signal. Such
499 a putative role for PfERC is supported by data which show that knockdown of PfERC
500 inhibits egress by preventing the breakdown of the PVM (Figure 3C-D).

501 A key enzyme that is required for initiating egress is the protease SUB1. Another
502 hypothesis we tested was if PfERC was required for the $Ca^{2+}$ dependent activity of SUB1.
503 This serine proteases plays a critical role in disruption of both the PVM and RBCM. It is
504 produced as an 82-kDa zymogen in the ER, where it rapidly self-processes into a 54-kDa
505 semi-proenzyme that remains associated with the cleaved prodomain, thus inhibiting its
506 activity (43). The autocatalytic activity of SUB1 is $Ca^{2+}$ dependent and therefore, it was
507 possible that PfERC was required for this autoprocessing event by providing the required
508 $Ca^{2+}$ to SUB1. This would explain the phenotypes observed during knockdown of PfERC
509 as they are similar to that seen when SUB1 is conditionally knocked out (29). However,
510 our data show only the second processing step of SUB1 that produces the mature, active
511 form of the protease (p54 to p47), is affected (Figure 5A-B and Supplementary Figure
512 4A). There is no effect on the $Ca^{2+}$ dependent autoprocessing of SUB1 (p83 to p54) that
513 occurs in the ER (Figure 5A-B and Supplementary Figure 4A). The processing of SUB1
514 from p54 to p47 occurs once it is trafficked out of the ER and putatively during secretion
515 of exoneme vesicles (25). This processing defect reduces the activity of SUB1 as it is

defective in processing its substrate, MSP1 (Figure 5A-D). This processing event happens after the secretion of SUB1 into the PV as MSP1 is a GPI-anchored protein on the membrane of merozoites (28). These data suggest that PfERC is required for secretion of exonemes, which is consistent with a role for PfERC in signal-dependent release of $Ca^{2+}$ from the ER.

A principal finding of these studies is the identification of the first protein in the ER of *P. falciparum* with a specific role in egress of malaria parasites from RBCs and potentially in the invasion of parasites into the RBC (Figures 2, 3, 5 and 6). These studies lay the foundation for understanding the vital and key role that ER-resident proteins play in the egress of human malaria parasites from their infected RBC and their re-entry into the host cell. Some studies have suggested that a key class of antimalarials containing endoperoxides, which includes the frontline antimalarial artemisinin, may target PfERC (59) and one of the transcriptomic responses of artemisinin-resistant parasites is the overexpression of PfERC (68). These data suggest that targeting PfERC, and thus egress, is a viable strategy for antimalarial drug development.

## Material and Methods

**Cell culture and transfections.** *Plasmodium* parasites were cultured in RPMI 1640 medium supplemented with Albumax I (Gibco) and transfected as described earlier (69-72). *T. gondii* tachyzoites were maintained in vitro by serial passage in Dulbecco's modified minimal essential media (DMEM) with 1% FBS, 2.5 µg/ml amphotericin B, and 100 µg/ml streptomycin. Host cells were human telomerase reverse transcriptase immortalized foreskin fibroblasts (hTERT) (73).

To generate PfERC-*glmS* and PfERC-*M9* parasites, a mix of two plasmids (50µg of each) was transfected in duplicate into 3D7 parasites. The plasmid mix contained pUF1-Cas9-guide (74) which contains the DHOD resistance gene, and pPfERC-HA-SDEL-*glmS* or pPfERC-HA-SDEL-*M9*, which are marker-free. Drug pressure was applied 48hrs after transfection, using 1µM (DSM1) (75), selecting only for Cas9 expression. DSM1 was then removed from the culturing medium once the parasites were detected in the culture, around 3 weeks post-transfection.

546 The *Δtgerc* knock-out line was generated by inserting the dihydrofolate reductase
547 (DHFR) gene into the first ~300 nucleotides of the *tgerc* gene to disrupt the coding
548 sequence. The CRISPR/Cas9 gene knockout method previously reported was used (39).
549 A fragment corresponding to the single guide RNA (sgRNA) using primers 1+2 was
550 cloned into pSAG1:CAS9::U6:sgUPRT (Addgene #54467) using the Q5 site-directed
551 mutagenesis kit (NEB). The resulting pSAG1:CAS9::U6:sgTgERC was co-transfected
552 with the DHFR cassette (in proportion 3:1) using primers 3+4 to tachyzoites of the RH
553 strain. After pyrimethamine selection (1 μM), parasites were sub-cloned by limiting dilution
554 and screened for positive clones by PCR using primers 5+6 shown in Table S1.
555
556 **Construction of PfERC plasmids.** Genomic DNA was isolated from *P. falciparum*
557 cultures using the QIAamp DNA blood kit (Qiagen). Constructs utilized in this study were
558 confirmed by sequencing. PCR products were inserted into the respective plasmids using
559 the In-Fusion cloning system (Clontech), the sequence- and ligation-independent cloning
560 (SLIC) method (71, 72), T4-ligation (New England BioLabs), or site-directed mutagenesis
561 using QuickChange (Agilent). To generate the pHA-SDEL-*glmS*/*M9* plasmid, primers 7+8
562 were used to add an SDEL sequence at the end of the HA tag in pHA-*glmS* and pHA-*M9*
563 plasmids (71, 72).
564 For the generation of the PfERC-*glmS*/*M9* conditional mutants, pHA-SDEL-
565 *glmS*/*M9* plasmid was used as a donor DNA template consisting of two homology regions
566 flanking the HA-SDEL tag and the *glmS* or *M9* sequence. To allow efficient genomic
567 integration of the pHA-SDEL-*glmS* and pHA-SDEL-*M9* donor plasmids, 800-bp
568 sequences were used for each homology region. The C-terminus of the *pferc* coding
569 region was PCR amplified from genomic DNA using primers 9+10 (containing the shield
570 mutation) and was inserted into pHA-SDEL-*glmS* and pHA-SDEL-*M9* using restriction
571 sites SacII and AfeI. The 3'UTR of *pferc* was PCR amplified from genomic DNA using
572 primers 11+12 and was inserted into pHA-SDEL-*glmS* and pHA-SDEL-*M9* (already
573 containing the C-terminus region) using restriction sites HindIII and NheI. For expression
574 of PfERC guide RNA, oligos 13+14 were inserted into pUF1-Cas9-guide as previously
575 described (74, 76). Briefly, pUF1-Cas9-guide was digested with BtgZI and annealed

oligos were inserted using the SLIC method. Primers 9+12 and primers 9+15 (which recognizes the *glmS*/*M9* sequence) were used for clone verification.

***Plasmodium* growth assays**. Asynchronous growth assays were done as described previously (71, 72). Briefly, 5mM glucosamine (GlcN) (Sigma) was added to the growth medium and parasitemia was monitored every 24hrs via flow cytometry using a CyAn ADP (Beckman Coulter) or CytoFLEX (Beckman Coulter) instrument and analyzed by FlowJo software (Treestar, Inc.). As required, parasites were subcultured to avoid high parasite density, and relative parasitemia at each time point was back-calculated based on actual parasitemia multiplied by the relevant dilution factors. One hundred percent parasitemia was determined as the highest relative parasitemia and was used to normalize parasite growth. Data were fit to exponential growth equations using Prism (GraphPad Software, Inc.).

To determine the ring:schizont ratio of PfERC-*glmS* and PfERC-*M9* parasites, 7.5mM GlcN was added to percoll isolated schizont-stage parasites and parasites were allowed to egress and reinvade fresh RBCs. Two hours later, 5% sorbitol +7.5mM GlcN was added to the invaded culture to lyse any remaining schizonts and isolate two-hour rings. The ring-stage parasites were grown again in media supplemented with GlcN. Then samples were taken at 44hrs, 48hrs, and 56hrs, and read by flow cytometry to determine the population of rings and schizonts present at those times using FlowJo software (Treestar, Inc.). To determine the development of each life cycle stage during the asexual lifecycle of PfERC-*glmS* and PfERC-*M9* parasites, 7.5mM was added to percoll isolated schizont-stage parasites and parasites were allowed to egress and reinvade fresh RBCs. Time points were then taken by blood smears and the percentage of the specific lifecycle stage was calculated as: $\%\ of\ stage = \frac{number\ of\ specific\ stage}{total\ number\ of\ parasites}$. Time 0hr is when GlcN was added. To determine the % amount of egressing or invading parasites, we took the % values of schizonts or rings at 44hrs and subtracted that number from % values of schizonts or rings at 12hrs later.

For growth assays using Compound 1, synchronized schizonts were grown with 7.5mM GlcN for about 48hrs. Then, schizonts were percoll isolated and incubated with Compound 1 for 4hrs and then removed by gently washing parasites twice with 1mL of

607 warm, complete RPMI. Parasites were resuspended with fresh media and RBCs and
608 samples were taken and read by flow cytometry. DNA content was determined using
609 Hoechst staining (ThermoFisher).
610
611 **Plaque assays.** Plaque assays were done as previously described (77). Two hundred
612 freshly egressed tachyzoites were used to infect a confluent monolayer of hTERT
613 fibroblasts followed by 7 days of growth. Monolayers were fixed and stained with 5x
614 crystal violet. Plaque sizes were analyzed with FIJI by measuring the area of fifteen
615 plaques per biological replicate. At least 3 biological experiments were done for wild type
616 control RH and TgERC knockout.
617
618 **Generation of TgERC antibody.** The *tgerc* gene (TgGT1_229480) was identified from
619 ToxoDB. Total RNA of the wild type strain (RH) was extracted from freshly lysed parasites
620 using Trizol® reagent (Sigma) following the manufacturer's instructions. The RNA sample
621 was further treated with DNAse I for 10 min at 37 °C (New England Biolabs) to remove
622 contaminating DNA. Four micrograms of purified mRNA were used to synthesize cDNA
623 using the superscript III first-strand synthesis system according to the manufacturer's
624 protocol (ThermoFisher Scientific-Life Technologies). *T. gondii* cDNA was used as a
625 template for amplifying the *tgerc* gene (~ 1 Kb) with the primers 16+17 (Table S1). The
626 PCR product was gel purified and cloned using the pET32 Ek/LIC vector system
627 (Novagen). The construct was sequenced and transformed into *E. coli* BL21(DE3)-
628 CodonPlus. Expression of the TgERC protein was induced for 3 h at 37°C with 0.4 mM
629 isopropyl-β-D-thiogalactopyranoside (IPTG). Cells were pelleted and resuspended in
630 equilibration/binding buffer (50 mM $Na_3PO4$, 300 mM NaCl, 10 mM Imidazole, and 1:500
631 protease inhibitor cocktail P-8849). Cells were then sonicated on ice for 80 seconds total
632 with amplitude set to 30% (Branson Digital Sonifier Model 250) and centrifuged at 12,000
633 rpm at 4°C for 20 min. The supernatant was filtered through a 0.45 µm cellulose acetate
634 filter (VWR) and the protein was purified using HisPur Ni-NTA chromatography following
635 instructions from the manufacturer. Unbound proteins were washed off with a total volume
636 of 12 ml of wash buffer (50 mM $Na_3PO_4$, 300 mM NaCl and 20 mM Imidazole) and the

637 TgERC recombinant protein was eluted with 5 ml of elution buffer (50 mM $Na_3PO_4$ ,300
638 mM NaCl and 250 mM Imidizole). Elution fractions were verified by SDS-PAGE.
639 Antibodies against the TgERC recombinant protein were generated in mice. Six
640 CD-1 mice (Charles River, Inc.) were intraperitoneally injected with 100 µg of purified
641 TgERC recombinant protein mixed 1:1 with complete Freund adjuvant. Mice were
642 boosted twice with 50 µg of antigen and the final serum was collected by cardiac puncture
643 after $CO_2$ euthanasia (IACUC protocol A2018 02-021-Y1-A0)
644
645 **Western blotting.** Western blotting for *Plasmodium* parasites was performed as
646 described previously (71, 72). Briefly, parasites were permeabilized selectively by
647 treatment with ice-cold 0.04% saponin in PBS for 10 min and pellets were collected for
648 detection of proteins with the parasite. For detection of MSP1, schizonts were isolated on
649 a Percoll gradient (Genesee Scientific) and whole-cell lysates were generated by
650 sonication. The antibodies used in this study were rat anti-HA (3F10; Roche, 1:3,000),
651 rabbit anti-HA (715500; Invitrogen, 1:100), rabbit anti-PfEF1α (from D. Goldberg,
652 1:2,000), mouse anti-plasmepsin V (from D. Goldberg, 1:400), rabbit anti-SUB1 (from Z.
653 Dou and M. Blackman, 1:10,000), rat anti-AMA1 (28G2; Alan Thomas via BEI Resources,
654 NIAID, NIH 1:500), mouse anti-MSP1 (12.4; European Malaria Reagent Repository,
655 1:500) and mouse anti-RAP1 (2.29; European Malaria Reagent Repository, 1:500). The
656 secondary antibodies that were used are IRDye 680CW goat anti-rabbit IgG and IRDye
657 800CW goat anti-mouse IgG (LICOR Biosciences) (1:20,000). The Western blot images
658 were processed using the Odyssey Clx LICOR infrared imaging system software (LICOR
659 Biosciences). Calculation of knockdown and processing ratios was determined by both
660 the Odyssey infrared imaging system software and ImageJ 1.8 (NIH).
661 For *T. gondii*, lysates were prepared by resuspending a pellet of 1 x $10^8$ tachyzoites
662 in 50 µl of Cell Lytic$^M$ lysis buffer containing 12.5 U benzonase and 1X protease cocktail
663 inhibitor (P8340 Sigma). The reaction was stopped with one volume of 2% SDS and 1
664 mM EDTA. Total lysates were boiled in Laemmli sample buffer (BioRad) (78).
665 Immunoblots were done following established protocols using polyclonal mouse anti-
666 TgERC serum (1:1,000). The Odyssey Clx LICOR system was used for detection, and
667 the secondary antibody was goat anti-mouse IRDye 800WC (1:10,000).

**Immunofluorescence microscopy.** For IFAs, cells were fixed as described previously (71, 72). The antibodies used for IFA were: rat anti-HA antibody (clone 3F10; Roche, 1:100), rat anti-PfGRP78 (MRA-1247; BEI Resources, NIAID, NIH 1:100), mouse anti-MSP1 (12.4; European Malaria Reagent Repository, 1:500), rat anti-AMA1 (28G2; Alan Thomas via BEI Resources, NIAID, NIH 1:500), and mouse anti-RAP1 (2.29; European Malaria Reagent Repository, 1:500). Secondary antibodies used were anti-rat antibody conjugated to Alexa Fluor 488 or 546 and anti-rabbit antibody conjugated to Alexa Fluor 488, (Life Technologies, 1:100). Cells were mounted on ProLong diamond with 4',6'-diamidino-2-phenylindole (DAPI) (Invitrogen) and imaged using a Delta-Vision II microscope system with an Olympus IX-71 inverted microscope using a 100x objective or an Elyra S1 SR-SIM microscope (Zeiss, Jena, Germany). Image processing, analysis, and display were performed using SoftWorx or Axiovision and Adobe Photoshop. Adjustments to brightness and contrast were made for display purposes.

For *T. gondii* IFAs, extracellular parasites were collected and purified as previously described (77). Parasites were washed once with buffer A with glucose (BAG, 116 mM NaCl, 5.4 mM KCl, 0.8 mM $MgSO_4$, 5.5 mM glucose and 50 mM HEPES, pH 7.4) and an aliquot with 2 x $10^4$ parasites was overlaid on a coverslip previously treated with poly-L-Lysine. Intracellular tachyzoites were grown on hTERT cells on coverslips previously infected with freshly lysed parasites. Both extracellular and intracellular parasites preparations were fixed with 2.5% paraformaldehyde for 20 min at room temperature (RT), permeabilized with 0.25% Triton X-100 and blocked with 3% bovine serum albumin (BSA). For co-localization studies parasites were exposed to primary antibodies mouse anti-TgERC 1:1000 and rabbit anti-GFP 1:800 after transfection with the P30-GFP-HDEL plasmid (79). The secondary antibodies were Alexa-Fluor488 goat-anti mouse and Alexa-Flour594 goat-anti rabbit at 1:1,000. Slides were examined using an Olympus IX-71 inverted fluorescence microscope with a photometric CoolSNAP HQ charge-coupled device (CCD) camera driven by DeltaVision software (Applied Precision).

**Invasion Rate Quantification.** To calculate the invasion rate, parasites were treated as described previously (47). Briefly, 7.5mM GlcN was added to percoll isolated schizont-

stage parasites and parasites were allowed to egress and reinvade fresh RBCs. 48hrs later, schizonts were percoll purified and incubated with 20μM E-64 (Sigma) at 37°C in an incubator for 7-8hrs. Once incubation was done, merozoites were isolated by gently resuspending and passing the schizonts through a 1.2μm Acrodisic Syringe Filter (PALL). Merozoites were spun at 2000xg for 5min, and then resuspended in 100μL of complete RMPI medium and added to a 1mL culture of uninfected RBCs at 2% hematocrit. Cultures were grown in a FluoroDish cell culture dish (World Precision Instruments) and gassed in a chamber for 20-24hrs. Invasion rate was then measured by the following equation: $IR = iRBC \cdot \left[\frac{RBC/\mu L}{Mz/\mu L}\right]$ where "*iRBC*" is the parasitemia 20-24hrs later, "*RBC/μL*" are the free RBCs used before addition of merozoites and "*Mz/μL*" are the merozoites found in the 100μL suspension used before adding to fresh RBCs. Values for these variables were acquired by flow cytometry (CytoFLEX Beckman Coulter) with cells stained with acridine orange. The data were normalized using the IR values for PfERC-*M9* merozoites as 100%.

**Transmission Electron Microscopy.** 7.5mM GlcN was added to percoll isolated schizont-stage parasites and parasites were allowed to egress and reinvade fresh RBCs. 48hrs later, parasites were percoll-isolated and then incubated with 20μM E-64 for 8hrs. After incubation, parasites were washed with 1X PBS and gently resuspended in 2.5% glutaraldehyde in 0.1M sodium cacodylate-HCl (Sigma) buffer pH 7.2 for 1hr at room temperature. Parasites were then rinsed in 0.1M Cacodylate-HCl buffer before agar-enrobing the cells in 3% Noble agar. Parasites were post fixed in 1% osmium tetroxide/0.1M Cacodylate-HCl buffer for 1 hour and rinsed in buffer and deionized water. Dehydration of the parasite samples was done with an ethanol series and then exposed to Propylene oxide before infiltration with Epon-Araldite. The blocks of parasites were trimmed, and sections were obtained using a Reichert Ultracut S ultramicrotome (Leica, Inc., Deerfield, IL). 60-70nm sections were placed on 200-mesh copper grids and post-stained with ethanolic uranyl acetate and Reynolds Lead Citrate. Grids were viewed with a JEOL JEM-1011 Transmission Electron Microscope (JEOL USA, Inc., Peabody, MA) using an accelerating voltage of 80 KeV. Images were acquired using an AMT XR80M

729 Wide-Angle Multi-Discipline Mid-Mount CCD Camera (Advanced Microscopy
730 Techniques, Woburn, MA).
731
732 **Scanning Electron Microscopy.** 7.5mM GlcN was added to percoll isolated schizont-
733 stage parasites and parasites were allowed to egress and reinvade fresh RBCs. 48hrs
734 later, parasites were percoll-isolated and then incubated with 2μM Compound 2 for 4
735 hours without shaking at 37°C in an incubator. After incubation, parasites were washed
736 twice with warm, complete RPMI + 7.5mM GlcN. Samples were taken immediately after
737 washing off Compound 2 and then 30min after and fixed as with TEM samples. Parasites
738 were rinsed with 0.1M Cacodylate-HCl buffer before placing on glass coverslips prepared
739 with 0.1% Poly-L-lysine. Parasites were allowed to settle onto the glass coverslips in a
740 moist chamber overnight and then post fixed in 1% osmium tetroxide/0.1M Cacodylate-
741 HCl buffer for 30 minutes. Cells on coverslips were rinsed three times in deionized water
742 and then dehydrated with an ethanol series. The glass coverslips were critical point dried
743 in an Autosamdri-814 Critical Point Dryer (Tousimis Research Corporation, Rockville,
744 MD), mounted onto aluminum pin stubs with colloidal paint, and sputter coated with gold-
745 palladium with a Leica EM ACE600 Coater (Leica Microsystems Inc., Buffalo Grove, IL).
746 Stubs were examined with the FE-SEM FEI Teneo (FEI, Inc., Hillsboro, OR) using the
747 secondary electron detector to obtain digital images.
748
749 **Calcium Measurements.** To measure $Ca^{2+}$ in PfERC mutants, knockdown was induced
750 on synchronized schizonts. After 48hrs, schizonts were percoll purified and permeabilized
751 selectively by treatment with ice-cold 0.04% saponin in PBS for 10 min. Isolated parasites
752 were then washed 2X with BAG Buffer (116mM NaCl, 5.4mM KCl, 0.8mM $MgSO_4 \cdot 7H_2O$,
753 50mM HEPES, 5.5mM Glucose) + 7.5mM GlcN and incubated with 10μM Fluo-4AM
754 (ThermoFisher) for 45min while rocking at 37°C. After incubation, cells were washed 2X
755 with BAG buffer + 7.5mM GlcN and immediately taken for fluorimetric measurements.
756 Fluorescence measurements were carried out in a cuvette (Sarstedt) containing parasites
757 suspended in 2.5 ml of BAG buffer and 100uM EGTA (Sigma). The cuvette was placed
758 in a Hitachi F-4500 fluorescence spectrophotometer and Fluo-4AM excitation was done
759 at 505 nm with emission read at 530 nm (80). Drugs and reagents were added via a

760 Hamilton syringe. Final concentration of CPA (Sigma) was 3 μM, and Ionomycin (Sigma)
761 at 2μM.

762 Loading of *Toxoplasma gondii* tachyzoites with Fura-2AM (ThermoFisher) was
763 done as previously described (40). Briefly, freshly collected parasites were washed twice
764 with BAG by centrifugation (706 g for 10 min) and resuspended at a final density of 1 x
765 $10^9$ parasites/ml in loading buffer (BAG plus 1.5% sucrose, and 5μM Fura-2AM). The
766 suspension was incubated for 26 min at 26 °C with mild agitation. Subsequently, parasites
767 were washed twice with BAG to remove extracellular dye, re-suspended to a final density
768 of 1 x $10^9$/ml in BAG and kept on ice. For fluorescence measurements, 2 x $10^7$
769 parasites/ml were placed in a cuvette with 2.5 ml of BAG buffer. Fluorescence
770 measurements were done in a Hitachi F-7000 fluorescence spectrophotometer using the
771 Fura-2AM conditions for excitation (340 and 380 nm) and emission (510 nm). The Fura-
772 2AM fluorescence response to $Ca^{2+}$ was calibrated from the ratio of 340/380 nm
773 fluorescence values after subtraction of the background fluorescence of the cells at 340
774 and 380 nm as described previously (81). The $Ca^{2+}$ release rate is the change in $Ca^{2+}$
775 concentration during the initial 20 s after compound addition (41).
776
777 **Acknowledgments**
778 We thank Michael Reese for comments on the manuscript; Dan Goldberg for comments
779 on the manuscript, anti Ef1α and anti-PMV anitbodies; The European Malaria Reagent
780 Repository for anti-MSP1 12.4 and anti-RAP1 2.29, antibodies; Alan Thomas and BEI
781 Resources NIAID, NIH for anti-AMA1 28G2 and anti-BiP antibodies; Zhicheng Dou and
782 Michael Blackman for anti-SUB1 antibody; Purnima Bhanot for Compound 1 and
783 Compound 2; Muthugapatti Kandasamy at the University of Georgia Biomedical
784 Microscopy Core, Julie Nelson at the CTEGD Cytomtetry Shared Resource Lab, and
785 Mary Ard from the Georgia Electron Microscopy for technical assistance; Michael
786 Cipriano for assistance with protein alignment. This work was supported by UGA Startup
787 funds and UGA Faculty Research Grant (FRG-SE0031) to V.M., and the US National
788 Institutes of Health (R21AI133322) to V.M. and S.N.J.M., and (T32AI060546) to M.A.F.
789
790

## References

1. Torgerson PR, Mastroiacovo P. The global burden of congenital toxoplasmosis: a systematic review. Bull World Health Organ. 2013;91(7):501-8.
2. Checkley W, White J,A.Clinton, Jaganath D, Arrowood MJ, Chalmers RM, Chen X, et al. A review of the global burden, novel diagnostics, therapeutics, and vaccine targets for cryptosporidium. Lancet Infect Dis. 2015; 15:85-94.
3. Liu L, Oza S, Hogan D, Chu Y, Perin J, Zhu J, et al. Global, regional, and national causes of under-5 mortality in 2000-15: an updated systematic analysis with implications for the Sustainable Development Goals. Lancet. 2016;388(10063):3027-35.
4. WHO. World Malaria Report 2017. Geneva: World Health Organization 2017
5. Dondorp AM, Nosten F, Yi P, Das D, Phyo AP, Tarning J, et al. Artemisinin resistance in Plasmodium falciparum malaria. N Engl J Med. 2009;361(5):455-67.
6. Mita T, Venkatesan M, Ohashi J, Culleton R, Takahashi N, Tsukahara T, et al. Limited geographical origin and global spread of sulfadoxine-resistant "dhps" alleles in Plasmodium falciparum populations. J Infect Dis. 2011(12):1980.
7. Roper C, Pearce R, Nair S, Sharp B, François Nosten, Anderson T. Intercontinental spread of pyrimethamine-resistant malaria. Science. 2004(5687):1124.
8. Gosling R, Lorenz vS. The future of the RTS,S/AS01 malaria vaccine: an alternative development plan. PLoS Medicine, 2016;13 :e1001994.
9. Donald RGK, Allocco J, Singh SB, Nare B, Salowe SP, Wiltsie J, et al. Toxoplasma gondii cyclic GMP-dependent kinase: chemotherapeutic targeting of an essential parasite protein kinase. Eukaryot Cell. 2002;1(3):317-28.
10. Christine RC, Hackett F, Strath M, Penzo M, Chrislaine Withers-Martinez, David AB, et al. Malaria parasite cGMP-dependent protein kinase regulates blood stage merozoite secretory organelle discharge and egress. PLoS Pathogens, 2013; 9(5):e1003344.
11. Brochet M, Collins MO, Smith TK, Thompson E, Sebastian S, Volkmann K, Schwach F, et al. Phosphoinositide metabolism links cGMP-dependent protein kinase G to essential $Ca^{2+}$ signals at key decision points in the life cycle of malaria parasites. PloS Biology, 2014; 12(3): e1001806

12. Hortua Triana MA, Márquez-Nogueras KM, Vella SA, Moreno SNJ. Calcium signaling and the lytic cycle of the Apicomplexan parasite Toxoplasma gondii. BBA - Molecular Cell Research. 2018; 1865: 1846-1856
13. Brochet M, Billker O. Calcium signalling in malaria parasites. Mol Microbiol. 2016; 100(3):397-408.
14. Holder A, Baker D, Baker DA, Taylor HM, Sicard A, Grainger M, et al. The malaria parasite cyclic GMP-dependent protein kinase plays a central role in blood-stage schizogony. Eukaryot Cell. 2010;9(1):37-45.
15. Hale VL, Watermeyer JM, Hackett F, Vizcay G, Ooij Cv, Thomas JA, et al. Parasitophorous vacuole poration precedes its rupture and rapid host erythrocyte cytoskeleton collapse in Plasmodium falciparum egress. Proc Natl Acad Sci USA. 2017; 114(13):3439-3444.
16. Absalon S, Blomqvist K, Rudlaff RM, DeLano TJ, Pollastri MP, Dvorin JD. Calcium-dependent protein kinase 5 Is required for release of egress-specific organelles in Plasmodium falciparum. MBio. 2018;9(1):e00130.
17. Glushakova S, Beck JR, Garten M, Busse BL, Nasamu AS, Tenkova-Heuser T, et al. Rounding precedes rupture and breakdown of vacuolar membranes minutes before malaria parasite egress from erythrocytes. Cell Microbiol. 2018; 20(10):e12868.
18. Garg S, Agarwal S, Chitnis CE, Singh S, Kumar S, Yazdani SS. Calcium-dependent permeabilization of erythrocytes by a perforin-like protein during egress of malaria parasites. Nat Commun. 2013;4: 1736
19. Lourido S, Moreno SNJ. The calcium signaling toolkit of the Apicomplexan parasites Toxoplasma gondii and Plasmodium spp. Cell Calcium. 2015;57(3):186-93.
20. Lourido S, Tang K, Sibley LD. Distinct signalling pathways control Toxoplasma egress and host-cell invasion. EMBO J. 2012;31(24):4524-34.
21. Yeoh S, O'Donnell RA, Koussis K, Dluzewski AR, Ansell KH, Osborne SA, et al. Subcellular discharge of a serine protease mediates release of invasive malaria parasites from host erythrocytes. Cell. 2007;131(6):1072-83.

22. Nasamu AS, Glushakova S, Russo I, Oksman BVA, Kim AS, Fremont DH, et al. Plasmepsins IX and X are essential and druggable mediators of malaria parasite egress and invasion. Science. 2017; 358(6362):518-522.
23. Pino P, Caldelari R, Mukherjee B, Vahokoski J, Klages N, Maco B, et al. A multistage antimalarial targets the plasmepsins IX and X essential for invasion and egress. Science. 2017; 358(6362):522-528.
24. Blackman MJ, Fujioka H, Stafford WHL, Sajid M, Clough B, Fleck SL, et al. A subtilisin-like protein in secretory organelles of Plasmodium falciparum merozoites. J Biol Chem. 1998; 273(36):23398-409.
25. Sajid M, Withers-Martinez C, Blackman MJ. Maturation and specificity of Plasmodium falciparum subtilisin-like protease-1, a malaria merozoite subtilisin-like serine protease. J Biol Chem. 2000; 275(1):631-41.
26. Tawk L, Kent R, Gorgette O, Mercereau-Puijalon O, Barale J, Lacroix C, et al. A key role for plasmodium subtilisin-like SUB1 protease in egress of malaria parasites from host hepatocytes. J Biol Chem. 2013;288(46):33336-46.
27. Das S, Hertrich N, Perrin AJ, Withers-Martinez C, Collins CR, Jones ML, et al. Processing of Plasmodium falciparum merozoite surface protein MSP1 activates a spectrin-binding function enabling parasite egress from RBCs. Cell Host Microbe. 2015;18(4):433-44.
28. Thomas JA, Tan MSY, Hackett F, Blackman MJ, Bisson C, Umrekar TR, et al. A protease cascade regulates release of the human malaria parasite Plasmodium falciparum from host red blood cells. Nat Microbiol. 2018;3(4):447-55.
29. Besteiro S, Lebrun M, Lamarque M, Besteiro S, Papoin J, Roques M, et al. The RON2-AMA1 interaction is a critical step in moving junction-dependent invasion by Apicomplexan Parasites. PLoS Pathogens. 2011;7(2): e1001276.
30. Paul AS, Egan ES, Duraisingh MT. Host-parasite interactions that guide red blood cell invasion by malaria parasites. Curr Opin Hematol. 2015;22(3):220-226.
31. Tomavo S, Slomianny C, Meissner M, Vern BC. Protein trafficking through the endosomal system prepares intracellular parasites for a home invasion. PLoS Pathogens. 2013; 9(10):e1003629.

881 32. Coffey MJ, Jennison C, Tonkin CJ, Boddey JA. Role of the ER and Golgi in protein
882 export by Apicomplexa. Curr Opin Cell Biol. 2016;41:18-24.
883 33. Greca N, Hibbs AR, Riffkin C, Foley M, Tilley L. Identification of an endoplasmic
884 reticulum-resident calcium-binding protein with multiple EF-hand motifs in asexual
885 stages of Plasmodium falciparum. Mol Biochem Parasitol. 1997;89(2):283-93.
886 34. Honoré B. The rapidly expanding CREC protein family: members, localization,
887 function, and role in disease. Bioessays. 2009;31(3):262-77.
888 35. Prommana P, Uthaipibull C, Wongsombat C, Kamchonwongpaisan S, Yuthavong Y,
889 Knuepfer E, et al. Inducible knockdown of Plasmodium gene expression using the
890 glmS ribozyme. PLoS ONE. 2013;8(8): e73783.
891 36. Salmon BL, Oksman A, Goldberg DE. Malaria parasite exit from the host
892 erythrocyte: a two-step process requiring extraerythrocytic proteolysis. Proc Natl
893 Acad Sci U S A. 2001; 98(1):271-6.
894 37. Sidik SM, Hackett CG, Tran F, Westwood NJ, Lourido S. Efficient genome
895 engineering of Toxoplasma gondii using CRISPR/Cas9. PLoS ONE. 2014;9(6):
896 e100450.
897 38. Shen B, Brown KM, Lee TD, Sibley LD. Efficient gene disruption in diverse strains of
898 Toxoplasma gondii using CRISPR/CAS9. MBio. 2014;5(3): e01114-14.
899 39. Moreno SNJ, Zhong L. Acidocalcisomes in Toxoplasma gondii tachyzoites. Biochem
900 J. 1996; 313(Pt2):655-9.
901 40. Pace DA, McKnight CA, Liu J, Jimenez V, Moreno SNJ. Calcium entry in
902 Toxoplasma gondii and its enhancing effect of invasion-linked traits. J Biol Chem.
903 2014;289(28):19637-47.
904 41. Alleva LM. Calcium regulation in the intraerythrocytic malaria parasite Plasmodium
905 falciparum. Molecular and biochemical parasitology. 2001;117(2):121-8.
906 42. Giganti D, Bouillon A, Tawk L, Robert F, Martinez M, Crublet E, et al. A novel
907 Plasmodium-specific prodomain fold regulates the malaria drug target SUB1
908 subtilase. Nat Commun. 2014;5:4833.
909 43. Goel VK, Li X, Chen H, Shih-Chun Liu, Chishti AH, Steven SO. Band 3 Is a host
910 receptor binding merozoite surface protein 1 during the Plasmodium falciparum
911 invasion of erythrocytes. Proc Natl Acad Sciences USA. 2003; 100(9):5164-9.

912 44. Li X, Chen H, Oo TH, Daly TM, Bergman LW, Shih-Chun Liu, et al. A co-ligand
913 complex anchors Plasmodium falciparum merozoites to the erythrocyte invasion
914 receptor b and 3. J Biol Chem. 2004;279(7):5765-71.
915 45. Baldwin MR, Li X, Hanada T, Liu S, Chishti AH. Merozoite surface protein 1
916 recognition of host glycophorin A mediates malaria parasite invasion of red blood
917 cells. Blood. 2015; 125(17):2704-11.
918 46. Boyle MJ, Wilson DW, Richards JS, Riglar DT, Tetteh K, Conway DJ, et al. Isolation
919 of viable Plasmodium falciparum merozoites to define erythrocyte invasion events
920 and advance vaccine and drug development. Proc Natl Acad Sciences USA. 2010;
921 107(32): 14378-83.
922 47. Lin CS, Uboldi AD, Epp C, Bujard H, Tsuboi T, Czabotar PE, et al. Multiple
923 Plasmodium falciparum merozoite surface protein 1 complexes mediate merozoite
924 binding to human erythrocytes. J Biol Chem. 2016;291(14):7703-15.
925 48. Bannister LH, Mitchell GH, Butcher GA, Dennis ED. Lamellar membranes
926 associated with rhoptries in erythrocytic merozoites of Plasmodium knowlesi: a clue
927 to the mechanism of invasion. Parasitology. 1986;92(pt2):291-303.
928 49. Riglar DT, Richard D, Wilson DW, Boyle MJ, Dekiwadia C, Turnbull L, et al. Super-
929 resolution dissection of coordinated events during malaria parasite invasion of the
930 human erythrocyte. Cell Host Microbe. 2011;9(1):9-20.
931 50. Cowman AF, Tonkin CJ, Tham W, Duraisingh MT. The molecular basis of
932 erythrocyte invasion by malaria parasites. Cell Host Microbe. 2017;22:232-45.
933 51. Howard RF, Schmidt CM. The secretary pathway of Plasmodium falciparum
934 regulates transport of p82/RAP-1 to the rhoptries. Mol Biochem Parasitol.
935 1995;74(1):43-54.
936 52. Howard RF, Narum D, Blackman M, Thurman J. Analysis of the processing of
937 Plasmodium falciparum rhoptry-associated protein 1 and localization of Pr86 to
938 schizont rhoptries and p67 to free merozoites. Mol Biochem Parasitol. 1998;
939 92(1):111-22.
940 53. Narum DL, Thomas AW. Differential localization of full-length and processed forms
941 of PF83/AMA-1 an apical membrane antigen of Plasmodium falciparum merozoites.
942 Mol Biochem Parasitol. 1994;67(1):59-68.

943 54. Howell SA, Withers-Martinez C, Kocken C, Thomas AW, Blackman MJ. Proteolytic
944 processing and primary structure of Plasmodium falciparum apical membrane
945 antigen-1. J Biol Chem. 2001;276(33):31311-20.
946 55. Bannister LH, Hopkins JM, Dluzewski AR, Margos G, Williams IT, Blackman MJ, et
947 al. Plasmodium falciparum apical membrane antigen 1 (PfAMA-1) is translocated
948 within micronemes along subpellicular microtubules during merozoite development.
949 J Cell Sci. 2003;116(18):3825-34.
950 56. Healer J, Tiriglia T, Hodder AN, Gemmill AW, Cowman AF. Functional analysis of
951 Plasmodium falciparum apical membrane antigen 1 utilizing interspecies domains.
952 Infect Immun. 2005; 73(4):2444-2451.
953 57. Santos JM, Josling G, Ross P, Joshi P, Orchard L, Campbell T, et al. Red blood cell
954 invasion by the malaria parasite is coordinated by the PfAP2-I transcription factor.
955 Cell Host Microbe. 2017;21(6): 731-741.e10.
956 58. Kim H, Morita M, Sanai H, Hiramoto A, Sato A, Wataya Y, et al. Plasmodium
957 falciparum endoplasmic reticulum-resident calcium binding protein is a possible
958 target of synthetic antimalarial endoperoxides, N-89 and N-251. J Proteome Res.
959 2012;11(12):5704-11.
960 59. Billker O, Lourido S, Sibley LD. Calcium-Dependent Signaling and Kinases in
961 Apicomplexan Parasites. Cell Host & Microbe. 2009;5(6):612-22.
962 60. Lagal V, Binder EM, Huynh M, Kafsack BFC, Harris PK, Diez R, et al. Toxoplasma
963 gondii protease TgSUB1 is required for cell surface processing of micronemal
964 adhesive complexes and efficient adhesion of tachyzoites. Cell Microbiol.
965 2010;12(12):1792-808.
966 61. Monerri NCS, Flynn HR, Campos MG, Hackett F, Koussis K, Withers-Martinez C, et
967 al. Global identification of multiple substrates for Plasmodium falciparum SUB1, an
968 essential malarial processing protease. Infect Immun. 2011;79(3):1086-1097.
969 62. Knuepfer E, Rug M, Klonis N, Tilley L, Cowman AF. Trafficking of the major
970 virulence factor to the surface of transfected P falciparum-infected erythrocytes.
971 Blood. 2005;105(10):4078-87.

63. Jung DH, Mo SH, Kim DH. Calumenin, a multiple EF-hands Ca2+-binding protein, interacts with ryanodine receptor-1 in rabbit skeletal sarcoplasmic reticulum. Biochem Biophys Res Commun. 2006;343(1):34-42.
64. Xu S, Xu Y, Chen L, Fang Q, Song S, Chen J, et al. RCN1 suppresses ER stress-induced apoptosis via calcium homeostasis and PERK-CHOP signaling. Oncogenesis. 2017 Mar 20,;6(3):e304.
65. Mazzorana M, Hussain R, Sorensen T. Ca-dependent folding of human calumenin. PLoS ONE. 2016;11(3): e0151547.
66. Yonezawa N, Suzuki N, Ban S, Itoh E, Chen S, Yonezawa N, et al. Calcium-dependent structural changes in human reticulocalbin-1. J Biochem. 2014;155(5):281-93.
67. Mok S, Ashley EA, Ferreira PE, Zhu L, Lin Z, Yeo T, et al. Population transcriptomics of human malaria parasites reveals the mechanism of artemisinin resistance. Science. 2015;347(6220):431-435.
68. Drew ME, Banerjee R, Uffman EW, Gilbertson S, Rosenthal PJ, Goldberg DE. Plasmodium food vacuole plasmepsins are activated by falcipains. J Biol Chem. 2008(19):12870-12876.
69. Russo I, Oksman A, Goldberg DE. Fatty acid acylation regulates trafficking of the unusual Plasmodium falciparum calpain to the nucleolus. Mol Microbiol. 2009; 72(1):229-245.
70. Cobb DW, Florentin A, Fierro MA, Krakowiak M, Moore JM, Muralidharan V. The exported chaperone PfHsp70x is dispensable for the Plasmodium falciparum intraerythrocytic life cycle. mSphere. 2017 Oct 25,;2(5):e00363-17.
71. Florentin A, Cobb DW, Fishburn JD, Cipriano MJ, Kim PS, Fierro MA, et al. PfClpC is an essential Clp chaperone required for plastid integrity and Clp protease stability in Plasmodium falciparum. Cell Reports. 2017; 21(7):1746-56.
72. Farwell DG, Shera KA, Koop JI, Bonnet GA, Matthews CP, Reuther GW, et al. Genetic and epigenetic changes in human epithelial cells immortalized by telomerase. Am J Pathol. 2000; 156(5):1537-47.

1001 73. Spillman NJ, Beck JR, Ganesan SM, Niles JC, Goldberg DE. The chaperonin TRiC
1002 forms an oligomeric complex in the malaria parasite cytosol. Cell Microbiol. 2017;
1003 19(6): e12719.
1004 74. Ganesan SM, Morrisey JM, Ke H, Painter HJ, Laroiya K, Phillips MA, et al. Yeast
1005 dihydroorotate dehydrogenase as a new selectable marker for Plasmodium
1006 falciparum transfection. MolBiochem Parasitol. 2011;177(1):29-34.
1007 75. Ghorbal M, Gorman M, Macpherson CR, Martins RM, Scherf A, Lopez-Rubio J.
1008 Genome editing in the human malaria parasite Plasmodium falciparum using the
1009 CRISPR-Cas9 system. Nat Biotechnol. 2014;32(8):819-21.
1010 76. Liu J, Pace D, Dou Z, King TP, Guidot D, Li ZH, et al. A vacuolar-H+-
1011 pyrophosphatase (TgVP1) is required for microneme secretion, host cell invasion,
1012 and extracellular survival of Toxoplasma gondii. Mol Microbiol. 2014;93(4):698-712.
1013 77. Laemmli UK. Cleavage of structural proteins during the assembly of the head of
1014 bacteriophage T4. Nature. 1970;227(5259):680-5.
1015 78. Hager KM, Striepen B, Tilney LG, Roos DS. The nuclear envelope serves as an
1016 intermediary between the ER and Golgi complex in the intracellular parasite
1017 Toxoplasma gondii. J Cell Sci. 1999;112(16):2631.
1018 79. Budu A, Gomes MM, Melo PM, El CM, Bagnaresi P, Azevedo MF, et al.
1019 Calmidazolium evokes high calcium fluctuations in Plasmodium falciparum. Cell
1020 Signal. 2016;28(3):125-35.
1021 80. Grynkiewicz G, Poenie M, Tsien RY. A new generation of Ca2+ indicators with
1022 greatly improved fluorescence properties. J Biol Chem. 1985;260(6):3440-50.
1023 81. Waterhouse AM, Procter JB, Martin DM, Clamp M, Barton GJ. Jalview Version 2-a
1024 multiple sequence alignment editor and analysis workbench. Bioinformatics. 2009;
1025 25(9):1189-91.

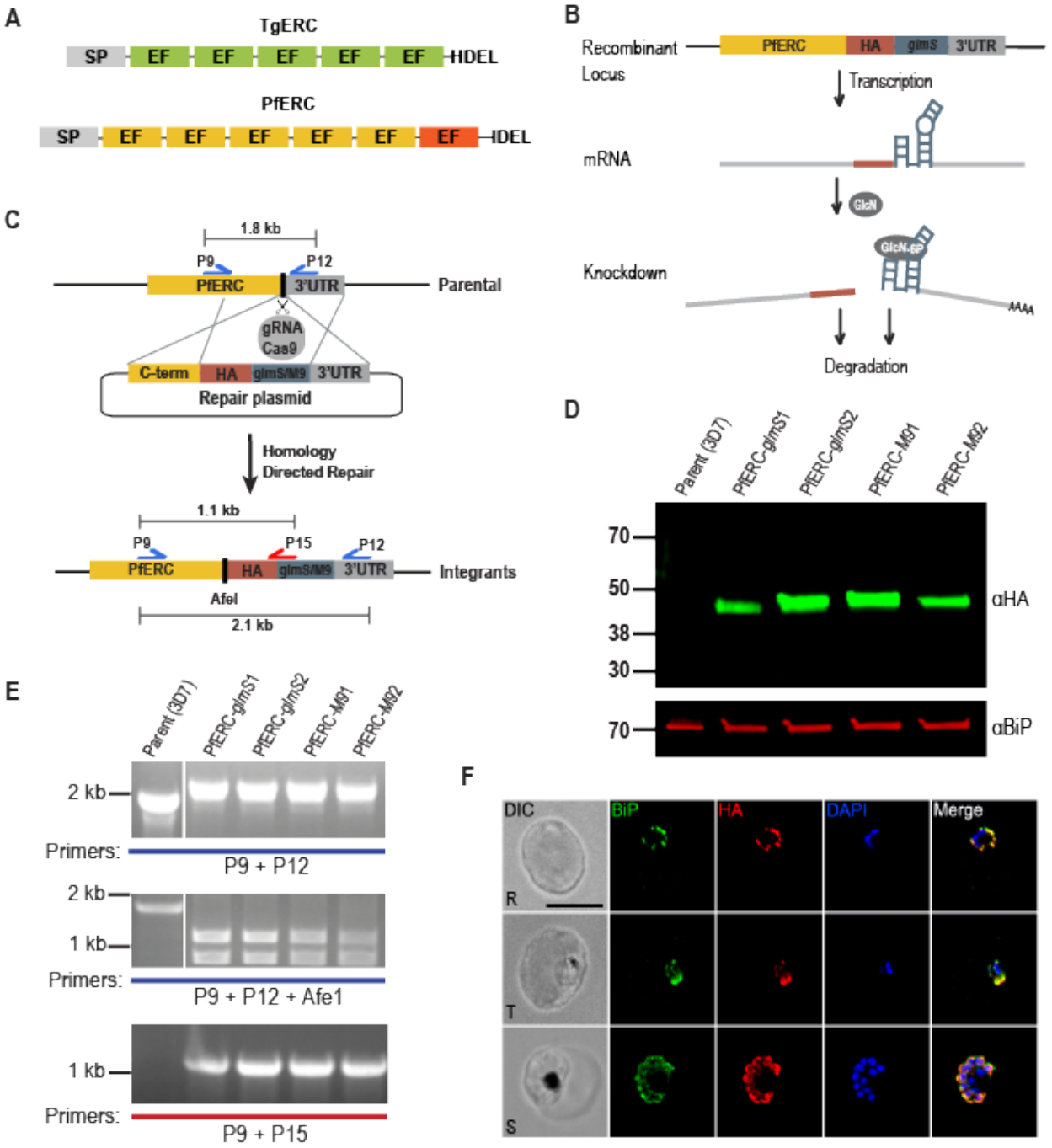


**Figure 1: Generating PfERC-*glmS*/*M9* mutant parasites.** (A) Schematic representation of the domain structure of PfERC and TgERC. Both proteins contain a signal peptide, 5 (TgERC) or 6 (PfERC) EF hands, and an ER-retention signal. (B) Mechanism of the conditional expression of PfERC using the *glmS* ribozyme system. This is an inactive ribozyme that is transcribed, but not translated, with the mRNA of a protein of interest. Addition of glucosamine (GlcN) leads to its phosphorylation within the

cell to glucosamine-6-phosphate (GlcN-6P). GlcN-6P binds to the transcribed PfERC-*glmS* mRNA and the *glmS* ribozyme is activated and cleaves itself from the mRNA. This leads to disassociation of the mRNA from its poly-A tail and leads to the degradation of target specific mRNA. The resulting decline in mRNA levels leads to reduced protein levels and, thus, loss of gene expression. As a control, we generated parasite lines containing a mutated version of the *glmS* ribozyme, called *M9*, which cannot cleave itself upon binding of GlcN. (C) Using the CRISPR/Cas9 system, we induced a double-stranded break in the PfERC locus that was repaired by a donor plasmid containing homology templates to the PfERC locus and appended a C-terminal 3XHA tag and a stop codon followed by the *glmS* or *M9* sequence to the targeted gene. The location of diagnostic primers used to demonstrate the repair of the locus via double cross-over homologous integration are also shown (P5, P8 and P11). (D) Western blot of lysates isolated from two independent clones and the parental line (3D7) probed with anti-HA antibodies show that the PfERC gene was tagged with HA in the mutants but not the parental line. PfBiP was the loading control. (E) PCR analysis of the generated mutants using specific primers (P5+P8; Table S1) in the C-terminus and 3'UTR of PfERC shows integration of the HA tag and *glms*/*M9* ribozymes into the PfERC locus. Modification of PfERC gene introduces an AfeI restriction enzyme site in this locus that is absent in the parental line. Digesting the PCR products (using AfeI) resulting from amplification using primers P5+P8 shows that AfeI is able to digest the PCR products from our mutants but not the parental line. PCR analysis using another primer pair (P5+P11) that sits on the *glmS*/*M9* sequence shows that amplification only occurs in the mutants but not in the parental line. (F) Representative IFA of PfERC-*M9* parasites showing that tagged PfERC localizes to the ER as shown with co-localization with the ER chaperone BiP in all asexual stages of the parasite. From left to right, the images are phase-contrast micrographs of parasites, parasites stained with anti-BiP antibody (green), parasites stained with anti-HA antibody (red), parasite nucleus stained with DAPI (blue), and fluorescence merge images of the parasites. Abbreviations: R, rings; T, trophozoites; S, schizonts. Scale bar, 5μm.

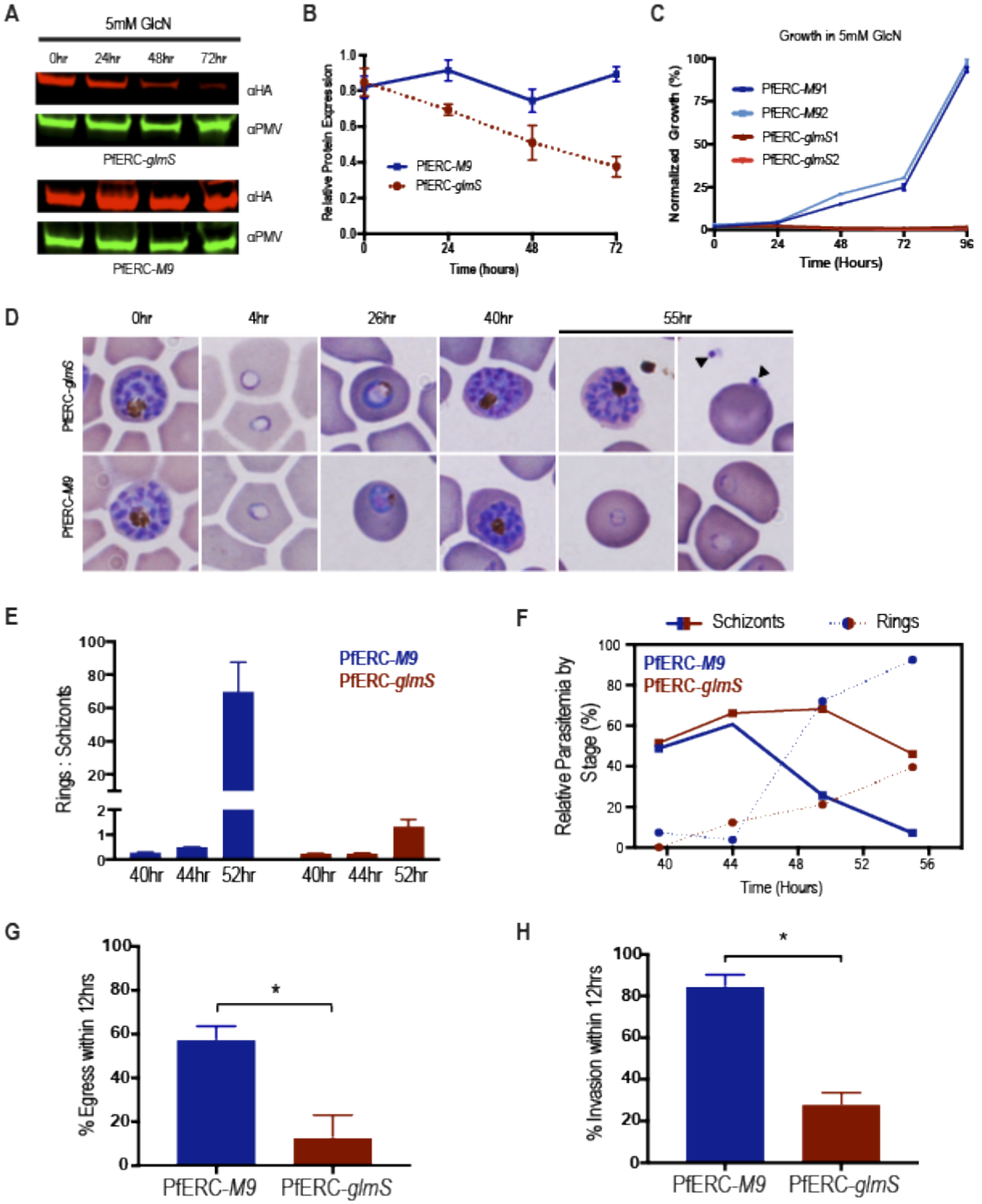


**Figure 2: PfERC mutants fail to transition from schizonts to rings.** (A) Western blot of parasite lysates isolated from PfERC-*glmS* and PfERC-*M9* parasites grown in the presence of 7.5 mM GlcN and probed with antibodies against HA (red) and against the ER-resident protease Plasmepsin V (PMV; green). One representative experiment out of

four is shown. (B) Quantification of the overall reduction in PfERC in PfERC-*glmS* and PfERC-*M9* parasites over time after addition of GlcN, as shown in (A). Data were normalized to the loading control (PMV) and are represented as mean ± SEM (n=4 biological replicates). (C) Growth curve of asynchronous PfERC-*glmS* and PfERC-*M9* clones grown in the presence of GlcN shows that PfERC is essential for asexual reproduction. Data are normalized to parasites grown without GlcN and are represented as the mean ± SEM (n=3 biological replicates). (D) Representative blood smears of synchronous PfERC-*glmS* and PfERC-*M9* parasites grown in the presence of GlcN (n=2 biological replicates). (E) Ring:schizont ratio of synchronous PfERC-*glmS* and PfERC-*M9* parasites taken at 40-52hrs post-addition of GlcN. Data are represented as the mean ± SEM (n=3 biological replicates). (F) The parasites shown in blood smears (D) were counted. The amount of each lifecycle stage (ring, trophozoite, schizont) was determined as a percentage of the total number of parasites for each time point. (G) The egress of PfERC-*glmS* or PfERC-*M9* parasites was quantified by determining the amount of schizonts in blood smears as in (D) present at 44hrs and at 56hrs. Egress was quantified using the following equation: (# of schizonts at 56h / # schizonts at 44h) x100. Data are represented as mean ± SEM (n=2 biological replicates; **P*<0.05, unpaired *t*-test). (H) Invasion of PfERC-*glmS* or PfERC-*M9* parasites was quantified by determining the amount of ring stages in blood smears as in (D) present at 44hrs and at 56hrs. This was quantified using the following equation: (# of rings at 44h / # rings at 56h) x100. Data are represented as mean ± SEM (n=2 biological replicates; **P*<0.05, unpaired *t*-test).

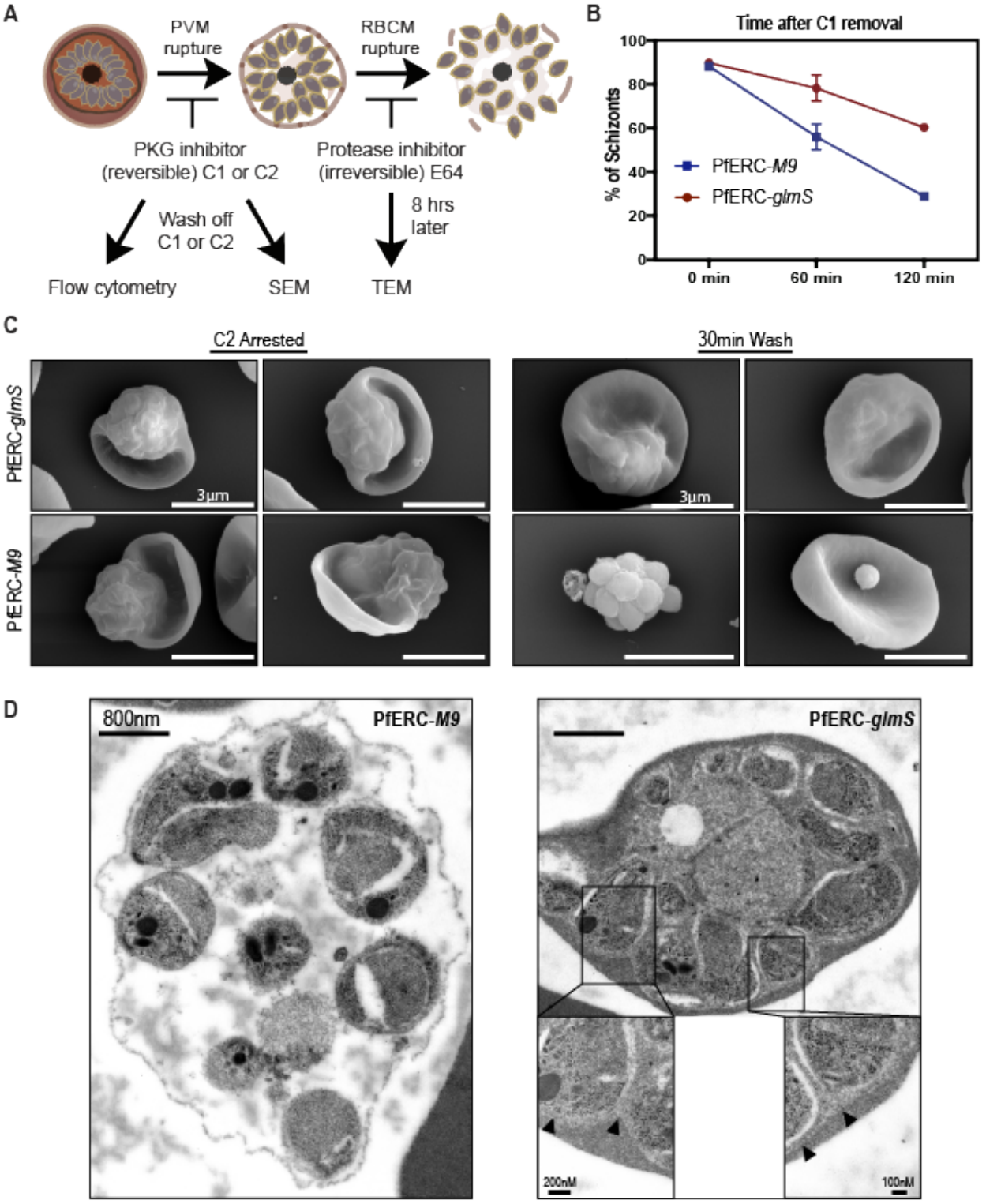


1086 **Figure 3: PfERC knockdown prevents PVM breakdown.** (A) Schematic showing the
1087 experimental layout to study the effect of PfERC knockdown using compounds that inhibit
1088 egress in parasites. Abbreviations: C1/2- PKG inhibitors, compound 1 or compound 2;

SEM- Scanning Electron Microscopy; TEM- Transmission Electron Microscopy. (B) As shown in (A), synchronized PfERC-*glmS* and PfERC-*M9* schizonts were observed by flow cytometry after removal of C1 (time 0hr). Schizonts were quantified as a percentage of the total amount of parasites as determined by flow cytometry. Data are represented as the mean ± SEM (n=3 biological replicates). (C) Representative SEM images of C2 arrested PfERC-*glmS* (n=2 biological replicates) and PfERC-*M9* (n=2 biological replicates) mutants fixed immediately after washing off C2 and after 30mins, as shown in (A). Scale bar, 800nm. (D) Representative TEM images of PfERC-*glmS* (n=2 biological replicates) and PfERC-*M9* (n=2 biological replicates) schizonts incubated with E-64, as shown in (A). PVM is marked by black arrowheads.

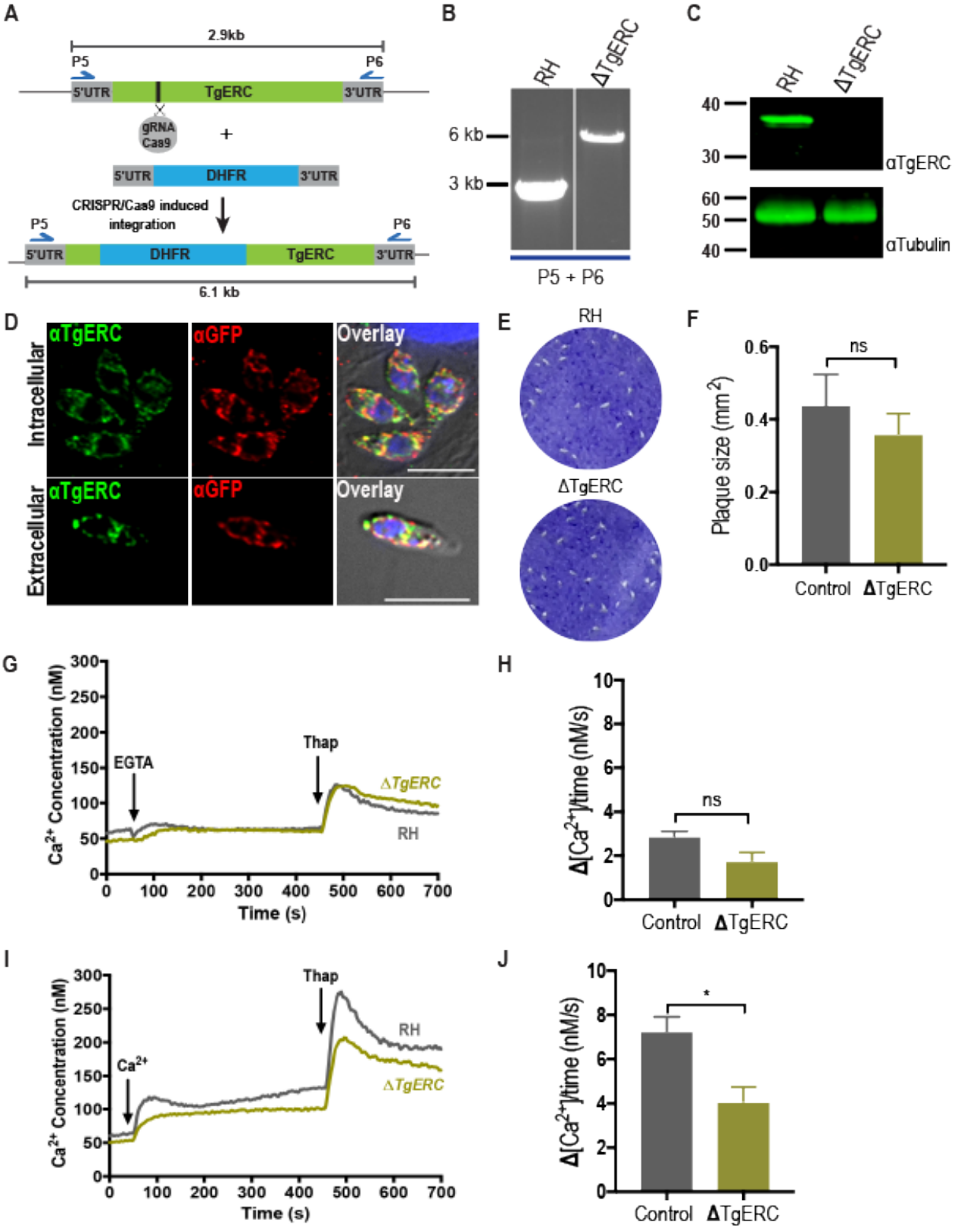


**Figure 4: Generation and characterization of TgERC mutants.** (A) Using CRISPR/Cas9, we generated *Δtgerc* mutants by introducing a DHFR cassette that

disrupted the open-reading frame of TgERC. (B) PCR analysis using primers that sit on the homology regions used for insertion showing amplification of the WT band (~3Kb) and insertion of the DHRF cassette as demonstrated by a higher product (~6Kb) in the mutants. (C) Western blot using generated antibodies against TgERC showing the presence of TgERC in the RH (WT) parasites but not in the *Δtgerc* mutants. αTubulin was used as the loading control. (D) IFAs of either extracellular or intracellular *Δtgerc* mutants transiently transfected with the P30-GFP-HDEL plasmid (79) which contains an ER-localized GFP. Left panel shows parasites probed with anti-TgERC antibodies, middle panel shows presence of transfected GFP, and right panel shows overlay of staining with DIC. Scale bar, 5μm. (E) Representative image of one plaque assay out of three biological replicates. (F) Quantification of plaque sizes between RH and *Δtgerc* parasites (n=3 biological replicates; n.s=non-significant, unpaired *t*-test). (G) Representative $Ca^{2+}$ tracings of RH and *Δtgerc* parasites treated with the extracellular $Ca^{2+}$ chelator EGTA and the SERCA pump inhibitor thapsigargin. (H) Quantification of the rate of $Ca^{2+}$ release of RH and *Δtgerc* parasites from (G) (n=3 biological replicates; n.s=non-significant, unpaired *t*-test). (I) Representative $Ca^{2+}$ tracings of RH and *Δtgerc* parasites treated with the extracellular $Ca^{2+}$ and thapsigargin. (J) Quantification of the rate of $Ca^{2+}$ release of RH and *Δtgerc* from (I) (n= 3 biological replicates, **P*<0.05, unpaired *t*-test).

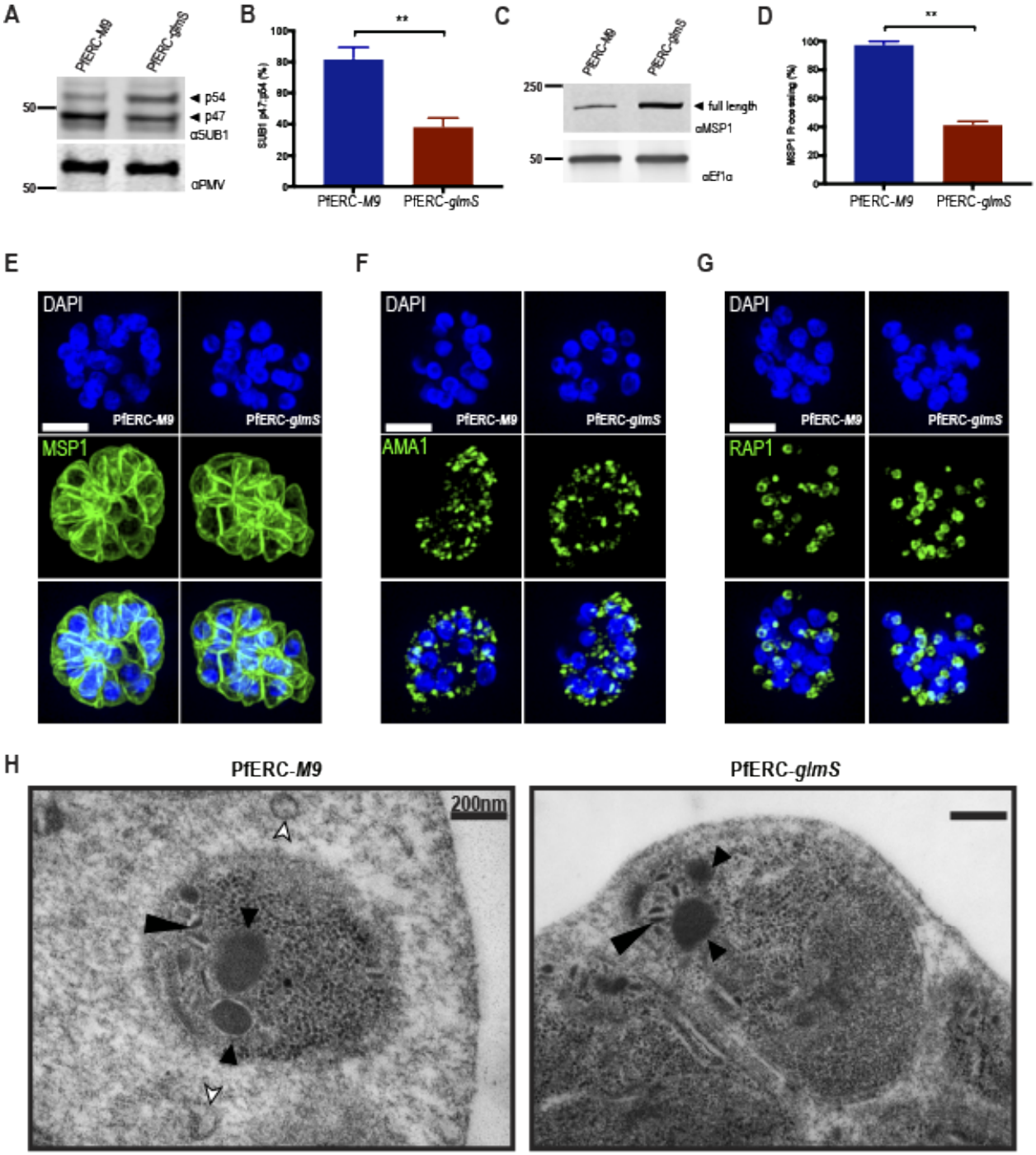


**Figure 5: PfERC knockdown inhibits SUB1 and MSP1 processing.** (A) Western blot of parasite lysates isolated from PfERC-*glmS* and PfERC-*M9* schizonts grown in the presence of GlcN for 48 hours and probed with anti-SUB1 antibodies (top panel) and against the ER-resident protease PMV (loading control, bottom panel). One representative experiment out of four is shown. The protein marker sizes that co-migrated

with the probed protein are shown on the left. (B) Quantification of the overall reduction in processing of SUB1 in PfERC-*glmS* and PfERC-*M9* parasites over time after addition of GlcN, as shown in (A). Data were normalized to the total SUB1 (processed + unprocessed) and are represented as mean ± SEM (n=4 biological replicates; ***P*<0.005 unpaired *t*-test). (C) Western blot of parasite lysates isolated from PfERC-*glmS* and PfERC-*M9* schizonts grown in the presence of GlcN for 48 hours and probed with anti-MSP1 antibodies (top panel) and against the anti-EF1α (loading control, bottom panel). One representative experiment out of two is shown. The protein marker sizes that co-migrated with the probed protein are shown on the left. (D) Quantification of the overall reduction in processing of MSP1 in PfERC-*glmS* and PfERC-*M9* parasites over time after addition of GlcN. Quantification of the overall reduction in MSP1 in PfERC-*glmS* and PfERC-*M9* parasites over time after addition of GlcN, as shown in (B). Data were normalized to the loading control (EF1α) and are represented as mean ± SEM (n=2 biological replicates; ***P*<0.005 unpaired *t*-test). (E-G) Representative Super-Resolution SIM images of PfERC-*glmS* and PfERC-*M9* schizonts stained with antibodies against MSP1, AMA1, and RAP1. From top to bottom, the images are parasites stained with anti-MSP1 (E), anti-AMA1 (F), anti-RAP1 (G) antibodies (green), parasite nucleus stained with DAPI (blue), and fluorescence merge images of the schizonts incubated with GlcN for 48hrs (n=2 biological replicates). Scale bar 2μm. (H) Representative TEM images of PfERC-*glmS* and PfERC-*M9* schizonts grown for 48hrs with GlcN and incubated with E-64 for 8 hours, as shown in Figure 3A (n=2 biological replicates). Small arrowheads point to rhoptries, large arrowheads to micronemes, and white arrowheads to PVM fragments (15). Scale bar, 200nm.

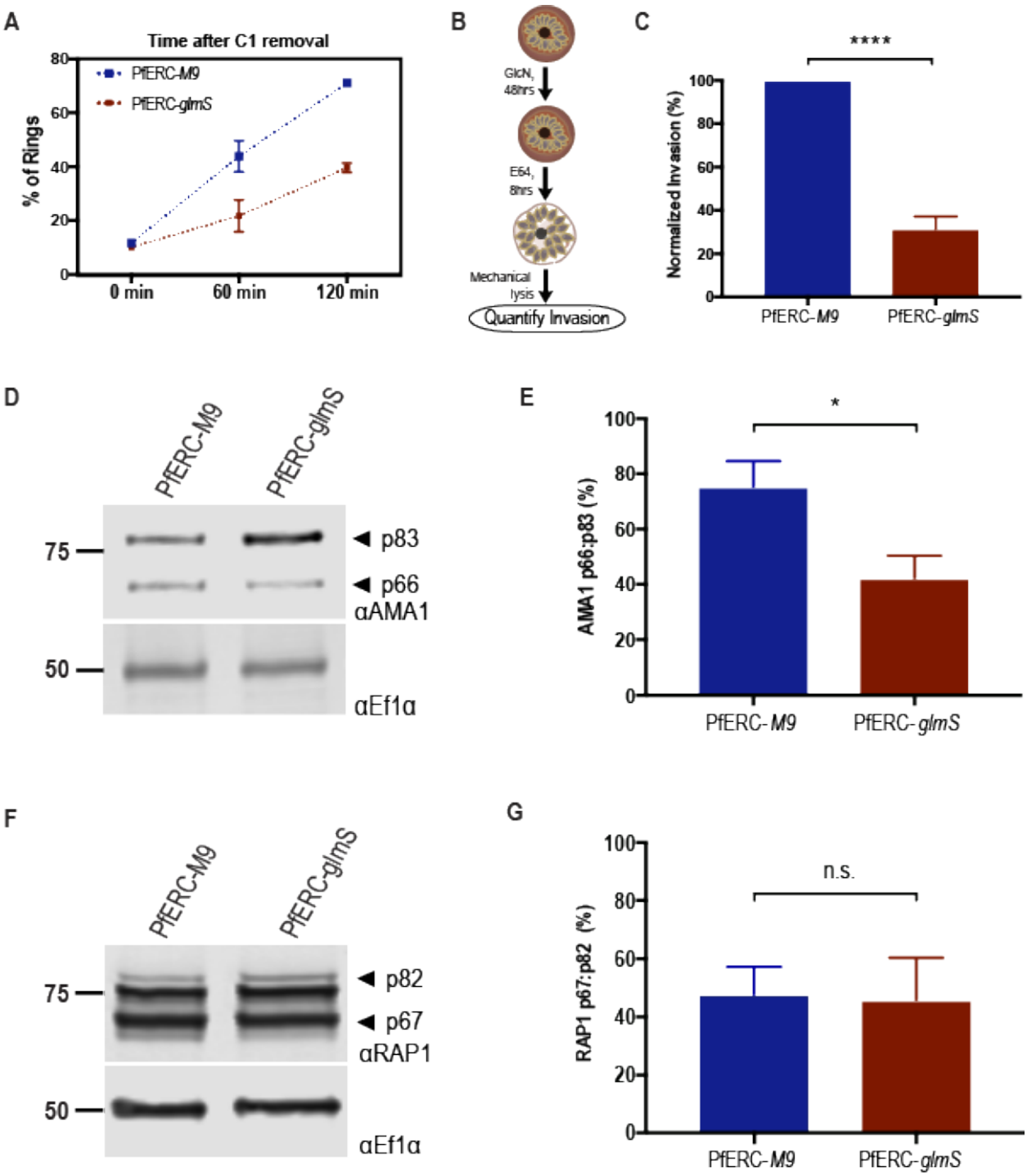


**Figure 6: PfERC knockdown prevents invasion of RBCs.** (A) As shown in Figure 4A, synchronized PfERC-*glmS* and PfERC-*M9* parasites were observed by flow cytometry after removal of C1 (time 0hr). Rings were quantified as a percentage of the total amount of parasites as determined by flow cytometry. Data are represented as the mean ± SEM (n=3 biological replicates). (B) Schematic showing the experimental layout to study the

effect of PfERC knockdown on invasion of merozoites into host RBCs. Merozoites were purified using mechanical lysis after 8hr incubation with E64. (C) Invasion rates of mechanically purified merozoites from PfERC-*glmS* and PfERC-*M9* parasites, as shown in (B), were quantified using flow cytometry (47). All replicates were normalized to PfERC-*M9* merozoites. Data are represented as mean ± SEM (n=7 biological replicates; ****$P$<0.0001, unpaired *t*-test). (D) Western blot of parasite lysates isolated from PfERC-*glmS* and PfERC-*M9* schizonts grown in the presence of GlcN for 48 hours and probed with anti-AMA1 antibodies (top panel) and anti- EF1αantibodies (loading control, bottom panel). One representative experiment out of eight is shown. The protein marker sizes that co-migrated with the probed protein are shown on the left. (E) Quantification of the overall reduction in processing of AMA1 in PfERC-*glmS* and PfERC-*M9* parasites over time after addition of GlcN, as shown in (D). Data were normalized to the total AMA1 (processed + unprocessed) and are represented as mean ± SEM (n=8 biological replicates; *$P$<0.05 unpaired *t*-test). (F) Western blot of parasite lysates isolated from PfERC-*glmS* and PfERC-*M9* schizonts grown in the presence of GlcN for 48 hours and probed with anti-RAP1 antibodies (top panel) and anti- EF1α antibodies (loading control, bottom panel). One representative experiment out of five is shown. The protein marker sizes that co-migrated with the probed protein are shown on the left. (G) Quantification of the overall reduction in processing of RAP1 in PfERC-*glmS* and PfERC-*M9* parasites over time after addition of GlcN, as shown in (F). Data were normalized to the total RAP1 (processed + unprocessed) and are represented as mean ± SEM (n=5 biological replicates; n.s=non-significant, unpaired *t*-test).

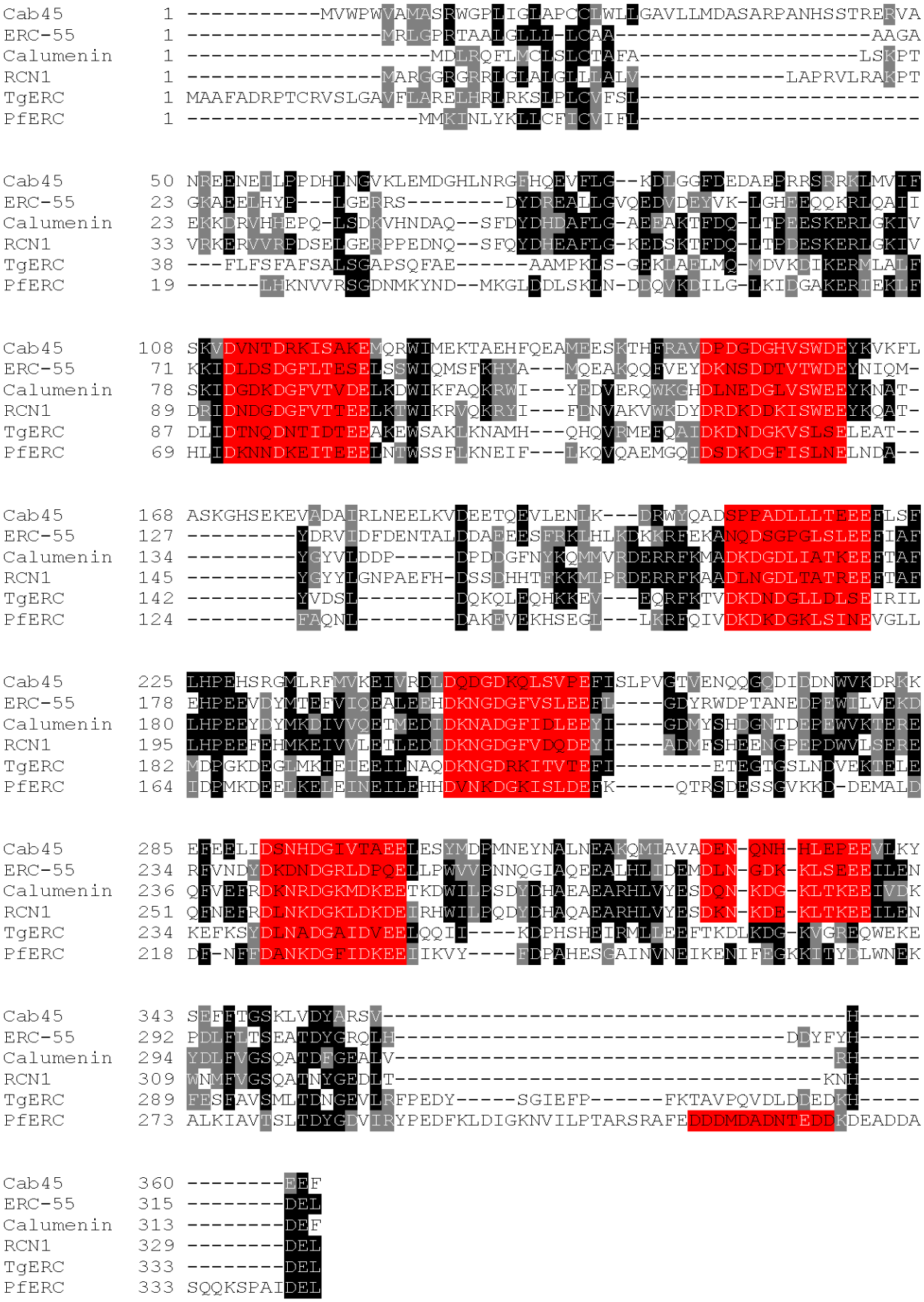

**Supplementary Figure 1:** Sequence alignment of TgERC and PfERC to other members of the CREC family of proteins using MUSCLE alignment, viewed using JalView Software (http://www.jalview.org/) and BOXSHADE (82). Alignment was done using the human homologs: Cab-45, ERC-55 (RCN2), Calumenin, and Reticulocalbin1 (RCN1). Identical residues are shaded in black, similar residues are shaded in gray, and EF-hands are highlighted in red.

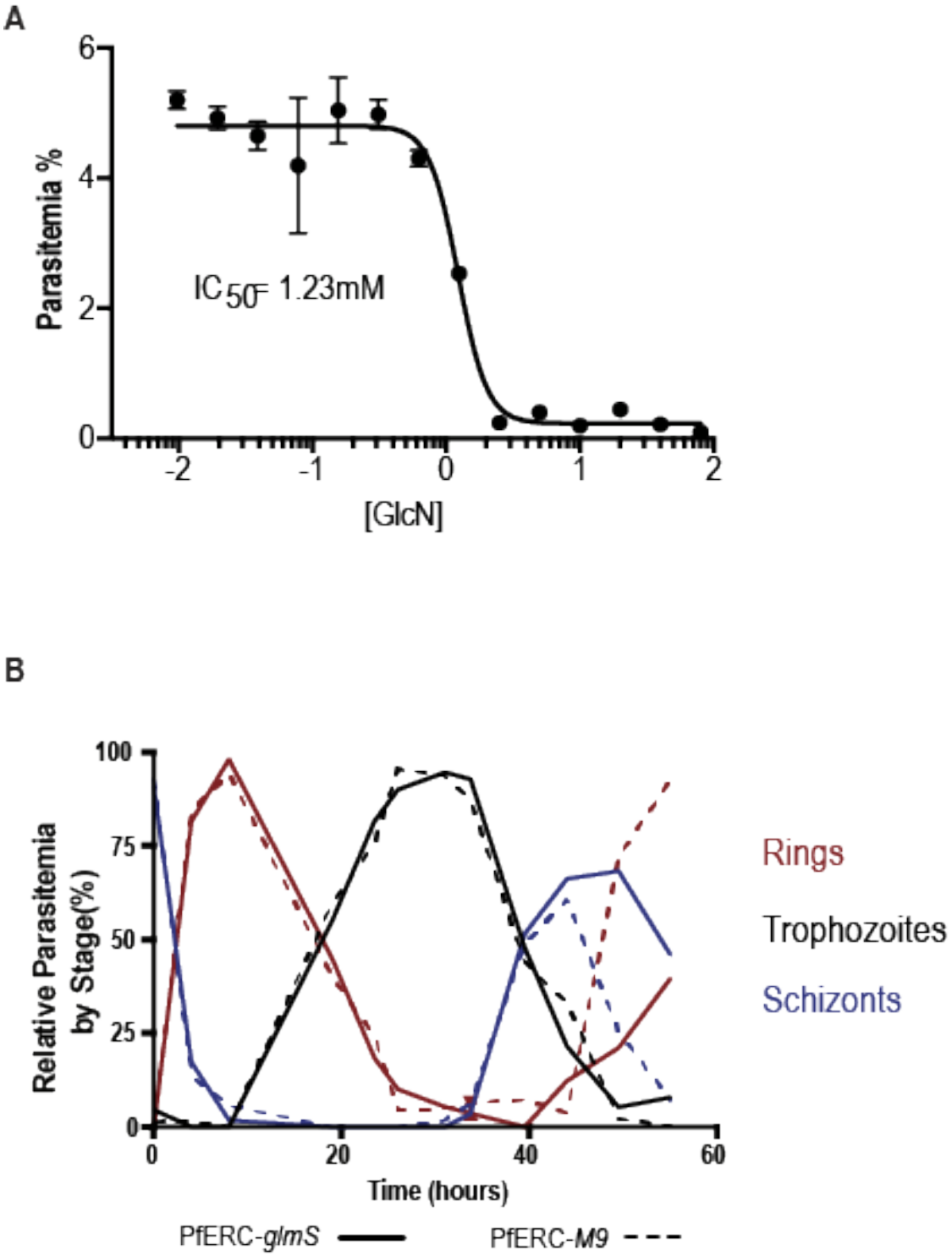


**Supplementary Figure 2:** Effect of PfERC knockdown on parasite growth. (A) Representative graph (one out of three) showing dose-dependent response of PfERC-*glmS*2 to GlcN. Asynchronous PfERC-*glmS* parasites were incubated in different concentrations of GlcN and growth after three days was assessed by flow cytometry. Data

1205 are represented as mean ± SEM of n=3 biological replicates. (B) Representative life cycle
1206 graph showing all stages from Figures 3D and 3F (n=2 biological replicates).

1207

1208

1209

1210

1211

1212

1213

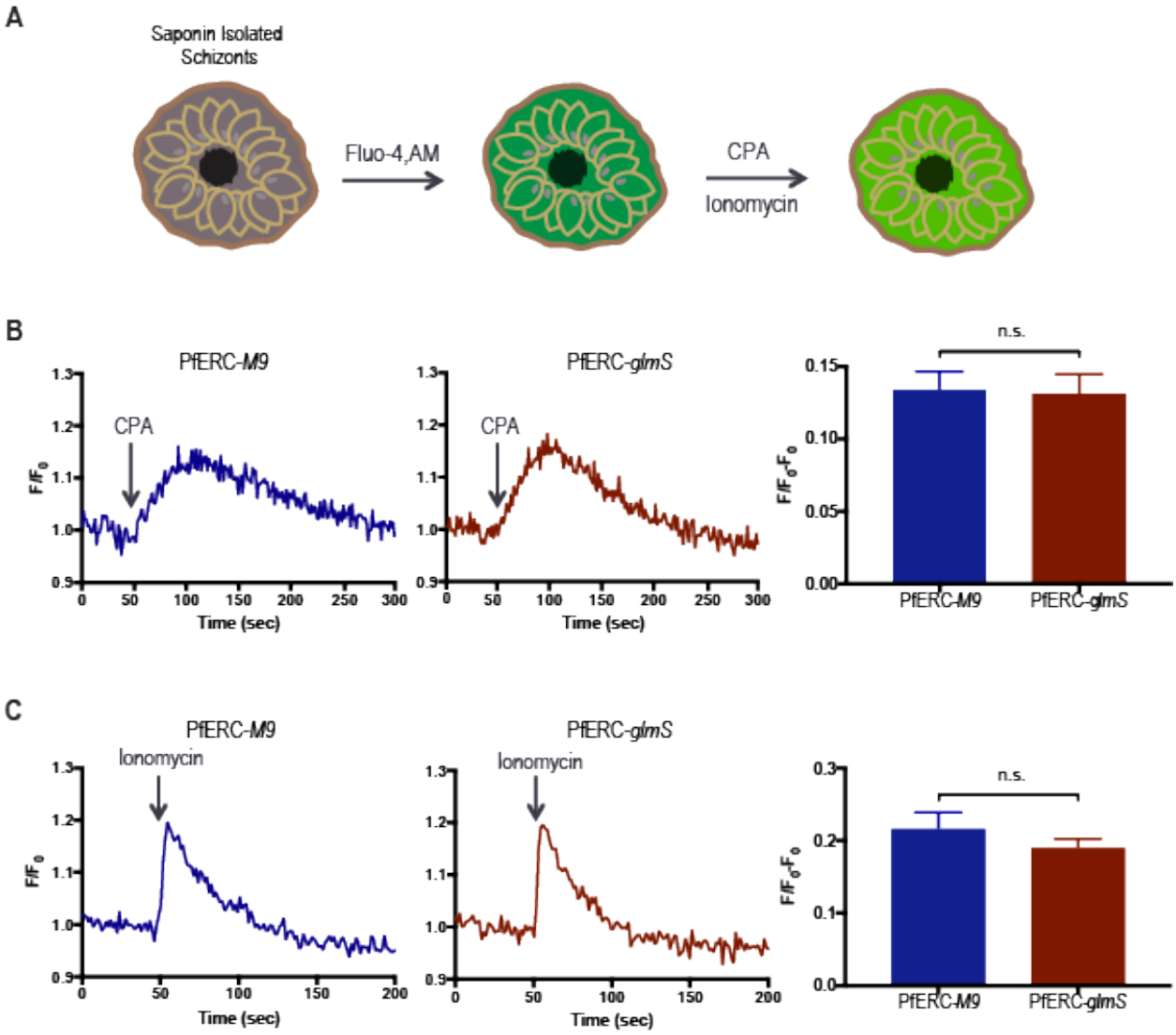


**Supplementary Figure 3:** Effect of PfERC knockdown on $Ca2^{2+}$ in the ER. (A) Experimental schematic showing how $Ca^{2+}$ measurements were done in PfERC-*glmS* and PfERC-*M9* mutants. Synchronized PfERC-*glmS* and PfERC-*M9* schizonts were incubated with GlcN for 48 hours and isolated using saponin lysis, which lyses the RBC membrane but leaves the PV intact. Abbreviations: CPA- cyclopiazoic acid (B) Representative fluorescence tracings after CPA addition to PfERC-*glmS* and PfERC-*M9* schizonts, isolated as in (A). Quantification was done by calculating the difference in fluorescence between the basal to the highest peak of fluorescence. Data are represented as the combined mean ± SEM (PfERC-*glmS;* n=15 biological replicates; PfERC-*M9;* n=9 biological replicates; n.s- non-significant, unpaired *t*-test). (C)

Representative fluorescence tracings after Ionomycin addition to PfERC-*glmS* and PfERC-*M9* schizonts, isolated as in (A). Quantification was done by calculating the difference in fluorescence between the basal to the highest peak of fluorescence. Data are represented as the combined mean ± SEM (PfERC-*glmS;* n=9 biological replicates; PfERC-*M9;* n=5 biological replicates; n.s- non-significant, unpaired *t*-test).

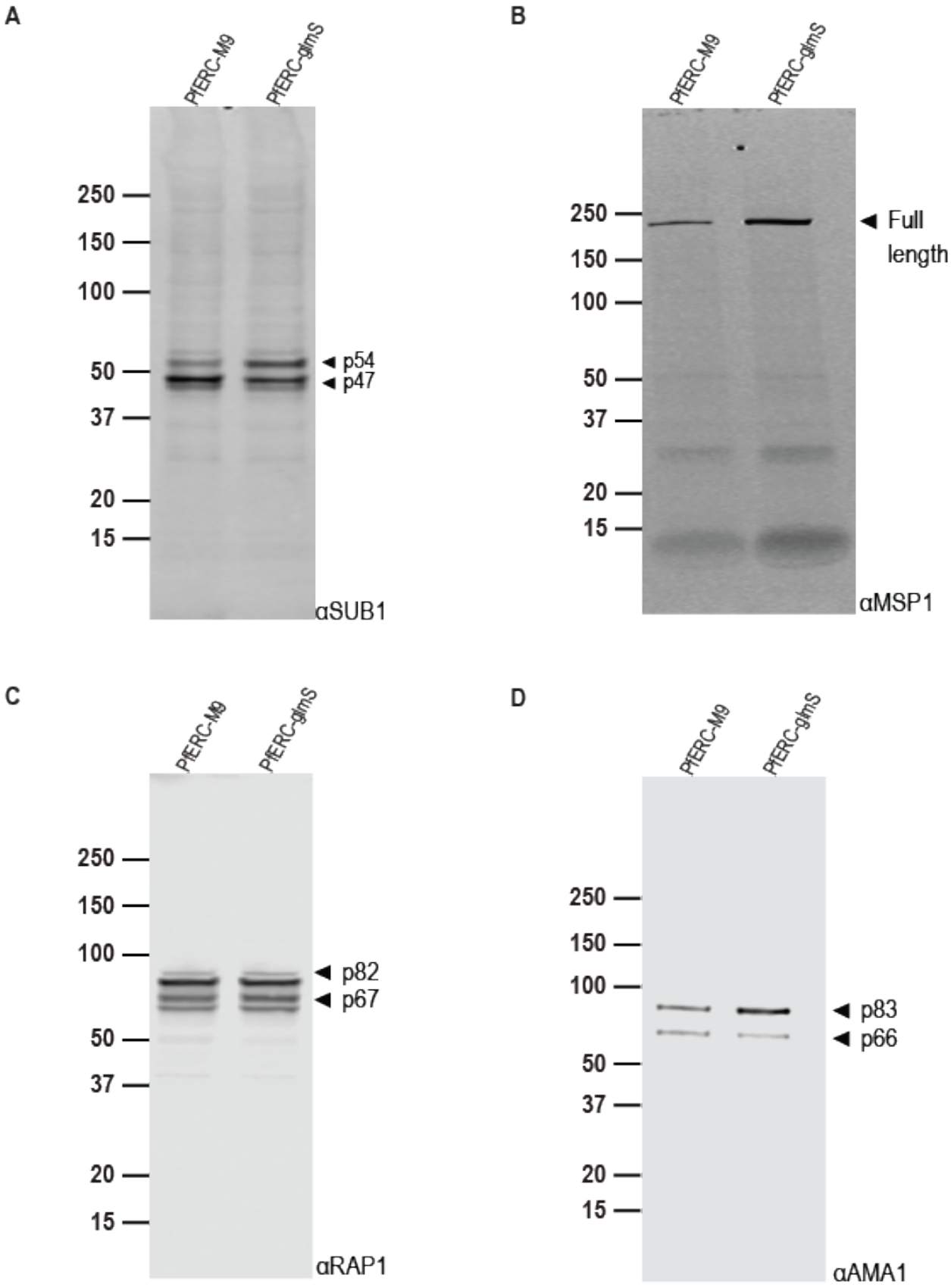


1230

**Supplementary Figure 4:** Representative whole-blot images of Western blots of lysates from PfERC-*glmS* and PfERC-*M9* schizonts incubated with GlcN for 48 hours, probed with anti-SUB1, anti-MSP1, anti-AMA1, and anti-RAP1 antibodies from Figures 5 and 6. The protein marker sizes that co-migrated with the probed protein are shown on the left.

1254 **Table S1:** Primers used in this study.

| Primer | Primer Sequence |
|---|---|
| 1 | GCGGCGATGCCCAAGTTGTCGTTTTAGAGCTAGAAATAGC |
| 2 | AACTTGACATCCCCATTTAC |
| 3 | CGACTGTTCCCCCCAATCAATTCTACTTTCGTCGCTTATCTCGAGAAAACAAAGCTTCGCCAGGCTGTAAATCC |
| 4 | CTCCTGTCCGCAGAAGCTCTGTACGTGTTCTCAACAACTAGCTCTTCATGTTCATCCTGCAAGTGCATAGAAGGAAAGTTG |
| 5 | TCCGACTCTCCAACGTGGTTGC |
| 6 | GCTGCTACACAGCACTCCCTG |
| 7 | CTGCAGGTCTGGACATTTAAAGTTCATCACTAGCGTAATCTGGAACATCG |
| 8 | CGATGTTCCAGATTACGCTAGTGATGAACTTTAAATGTCCAGACCTGCAG |
| 9 | AATTCGCCCTTTCCGCGGAGAATAGAAAAATTATTTCATTTGATAGATAAAAACAATGAT |
| 10 | TGGGTAACTAGTAGCGCTTAATTCATCAATTGCTGGGGATTTTTGTTGCGATGCATCGTC |
| 11 | ATGATCTTGCCGGCAAGCTTTTTATATAAACATATTTTTTTTTTTTTTAACATAAAGGG |
| 12 | CCTTGAGCTCGCTAGCGACAAATTGGATAGATAATAGGGGGTACAAATATACATAC |
| 13 | AAGTATATAATATTCAATTGCTGGGGATTTTTGTGTTTTAGAGCTAGAA |
| 14 | TTCTAGCTCTAAAACACAAAAATCCCCAGCAATTGAATATTATATACTTA |
| 15 | GCAAGATCATGTGATTTCTCTTTGTTCAAGGAGTCACCCCC |
| 16 | GACGACGACAAGATAATGGCGGCCTTCGCAGACAG |
| 17 | GAGGAGAAGCCCGGTCAGTTCATCGTGTTTGTCTTCGTCGTCG |

1255

1256